Living Rev. Solar Phys., **7**, (2010), 1
http://www.livingreviews.org/lrsp-2010-1

LIVING REVIEWS
in solar physics

The Solar Cycle

David H. Hathaway
Mail Code VP62,
NASA Marshall Space Flight Center,
Huntsville, AL 35812, U.S.A.
email: david.hathaway@nasa.gov
http://solarscience.msfc.nasa.gov/

Accepted on 21 February 2010
Published on 2 March 2010

Abstract

The Solar Cycle is reviewed. The 11-year cycle of solar activity is characterized by the rise and fall in the numbers and surface area of sunspots. We examine a number of other solar activity indicators including the 10.7 cm radio flux, the total solar irradiance, the magnetic field, flares and coronal mass ejections, geomagnetic activity, galactic cosmic ray fluxes, and radioisotopes in tree rings and ice cores that vary in association with the sunspots. We examine the characteristics of individual solar cycles including their maxima and minima, cycle periods and amplitudes, cycle shape, and the nature of active latitudes, hemispheres, and longitudes. We examine long-term variability including the Maunder Minimum, the Gleissberg Cycle, and the Gnevyshev–Ohl Rule. Short-term variability includes the 154-day periodicity, quasi-biennial variations, and double peaked maxima. We conclude with an examination of prediction techniques for the solar cycle.

Imprint / Terms of Use

Living Reviews in Solar Physics is a peer reviewed open access journal published by the Max Planck Institute for Solar System Research, Max-Planck-Str. 2, 37191 Katlenburg-Lindau, Germany. ISSN 1614-4961.

Because a *Living Reviews* article can evolve over time, we recommend to cite the article as follows:

David H. Hathaway,
"The Solar Cycle",
Living Rev. Solar Phys., **7**, (2010), 1. [Online Article]: cited [<date>],
http://www.livingreviews.org/lrsp-2010-1

The date given as <date> then uniquely identifies the version of the article you are referring to.

Article Revisions

Living Reviews supports two different ways to keep its articles up-to-date:

Fast-track revision A fast-track revision provides the author with the opportunity to add short notices of current research results, trends and developments, or important publications to the article. A fast-track revision is refereed by the responsible subject editor. If an article has undergone a fast-track revision, a summary of changes will be listed here.

Major update A major update will include substantial changes and additions and is subject to full external refereeing. It is published with a new publication number.

For detailed documentation of an article's evolution, please refer always to the history document of the article's online version at http://www.livingreviews.org/lrsp-2010-1.

Contents

List of Tables

1 Introduction

Solar activity rises and falls with an 11-year cycle that affects us in many ways. Increased solar activity includes increases in extreme ultraviolet and x-ray emissions from the Sun which produce dramatic effects in the Earth's upper atmosphere. The associated atmospheric heating increases both the temperature and density of the atmosphere at many spacecraft altitudes. The increase in atmospheric drag on satellites in low Earth orbit can dramatically shorten the lifetime of these valuable assets (cf. Pulkkinen, 2007).

Increases in the number of solar flares and coronal mass ejections (CMEs) raise the likelihood that sensitive instruments in space will be damaged by energetic particles accelerated in these events. These solar energetic particles (SEPs) can also threaten the health of both astronauts in space and airline travelers in high altitude, polar routes.

Solar activity apparently affects terrestrial climate as well. Although the change in the total solar irradiance seems too small to produce significant climatic effects, there is good evidence that, to some extent, the Earth's climate heats and cools as solar activity rises and falls (cf. Haigh, 2007).

There is little doubt that the solar cycle is magnetic in nature and produced by dynamo processes within the Sun. Here we examine the nature of the solar cycle and the characteristics that must be explained by any viable dynamo model (cf. Charbonneau, 2005).

2 The Solar Cycle Discovered

Sunspots (dark patches on the Sun where intense magnetic fields loop up through the surface from the deep interior) were almost certainly seen by prehistoric humans viewing the Sun through hazy skies. The earliest actual recordings of sunspot observations were from China over 2000 years ago (Clark and Stephenson, 1978; Wittmann and Xu, 1987). Yet, the existence of spots on the Sun came as a surprise to westerners when telescopes were first used to observe the Sun in the early 17th century. This is usually attributed to western philosophy in which the heavens and the Sun were thought to be perfect and unblemished (cf. Bray and Loughhead, 1965; Noyes, 1982).

The first mention of possible periodic behavior in sunspots came from Christian Horrebow who wrote in his 1776 diary:

> "Even though our observations conclude that changes of sunspots must be periodic, a precise order of regulation and appearance cannot be found in the years in which it was observed. That is because astronomers have not been making the effort to make observations of the subject of sunspots on a regular basis. Without a doubt, they believed that these observations were not of interest for either astronomy or physics. One can only hope that, with frequent observations of periodic motion of space objects, that time will show how to examine in which way astronomical bodies that are driven and lit up by the Sun are influenced by sunspots." (Wolf, 1877, translation by Elke Willenberg)

2.1 Schwabe's discovery

Although Christian Horrebow mentions this possible periodic variation in 1776 the solar (sunspot) cycle was not truly discovered until 1844. In that year Heinrich Schwabe reported in *Astronomische Nachrichten* (Schwabe, 1844) that his observations of the numbers of sunspot groups and spotless days over the previous 18-years indicated the presence of a cycle of activity with a period of about 10 years. Figure 1 shows his data for the number of sunspot groups observed yearly from 1826 to 1843.

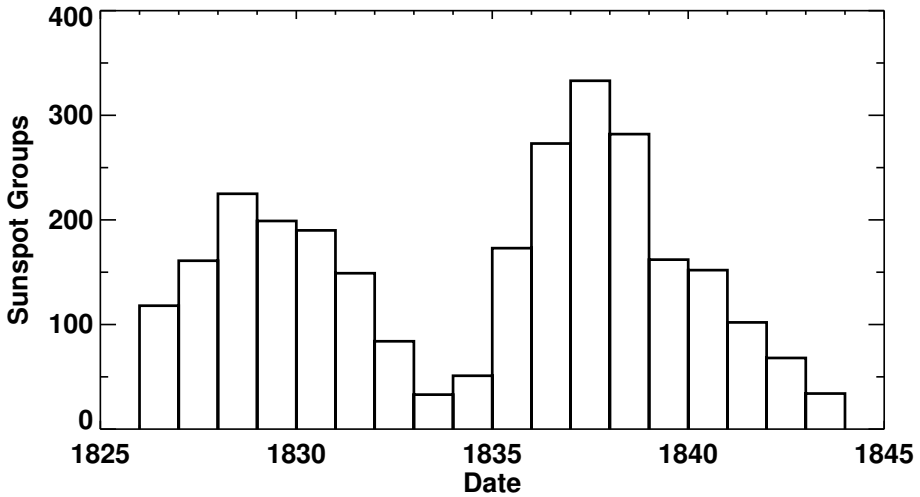

Figure 1: Sunspot groups observed each year from 1826 to 1843 by Heinrich Schwabe (1844). These data led Schwabe to his discovery of the sunspot cycle.

2.2 Wolf's relative sunspot number

Schwabe's discovery was probably instrumental in initiating the work of Rudolf Wolf (first at the Bern Observatory and later at Zürich) toward acquiring daily observations of the Sun and extending the records to previous years (Wolf, 1861). Wolf recognized that it was far easier to identify sunspot groups than to identify each individual sunspot. His "relative" sunspot number, R, thus emphasized sunspot groups with

$$R = k\,(10\,g + n) \tag{1}$$

where k is a correction factor for the observer, g is the number of identified sunspot groups, and n is the number of individual sunspots. These Wolf, Zürich, or International Sunspot Numbers have been obtained daily since 1849. Wolf himself was the primary observer from 1848 to 1893 and had a personal correction factor $k = 1.0$. The primary observer has changed several times (Staudacher from 1749 to 1787, Flaugergues from 1788 to 1825, Schwabe from 1826 to 1847, Wolf from 1848 to 1893, Wolfer from 1893 to 1928, Brunner from 1929 to 1944, and Waldmeier from 1945 to 1980). The Swiss Federal Observatory continued to provide sunspot numbers through 1980. Beginning in 1981 and continuing through the present, the International Sunspot Number has been provided by the Royal Observatory of Belgium with Koeckelenbergh as the primary observer (Solar Influences Data Analysis Center - SIDC). Both Wolf and Wolfer observed the Sun in parallel over a 16-year period. Wolf determined that the k-factor for Wolfer should be $k = 0.60$ by comparing the sunspot numbers calculated by Wolfer to those calculated by Wolf over the same days. In addition to these primary observers there were many secondary and tertiary observers whose observations were used when those of the primary were unavailable. The process was changed from using the numbers from a single primary/secondary/tertiary observer to using a weighted average of many observers when the Royal Observatory of Belgium took over the process in 1981.

2.3 Wolf's reconstruction of earlier data

Wolf extended the data back to 1749 using the primary observers along with many secondary observers but much of that earlier data is incomplete. Wolf often filled in gaps in the sunspot observations using geomagnetic activity measurements as proxies for the sunspot number. It is well recognized that the sunspot numbers are quite reliable since Wolf's time but that earlier numbers are far less reliable. The monthly averages of the daily numbers are shown in Figure 2.

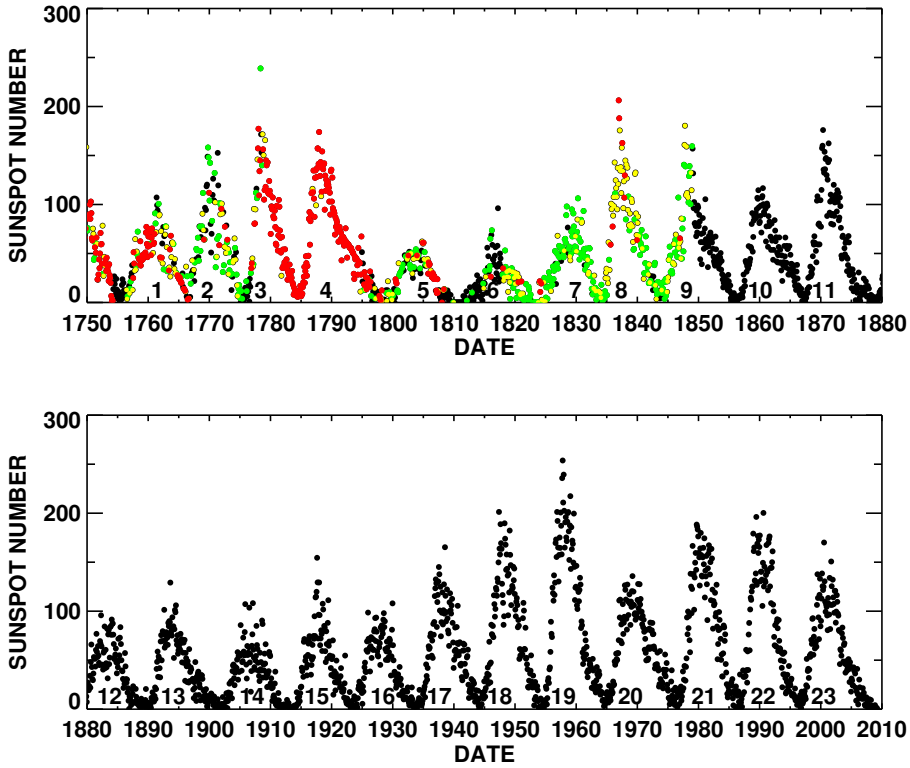

Figure 2: Monthly averages of the daily International Sunspot Number. This illustrates the solar cycle and shows that it varies in amplitude, shape, and length. Months with observations from every day are shown in black. Months with 1 – 10 days of observation missing are shown in green. Months with 11 – 20 days of observation missing are shown in yellow. Months with more than 20 days of observation missing are shown in red. [Missing days from 1818 to the present were obtained from the International daily sunspot numbers. Missing days from 1750 to 1818 were obtained from the Group Sunspot Numbers and probably represent an over estimate.]

3 Solar Activity Data

3.1 Sunspot numbers

The International Sunspot Number is the key indicator of solar activity. This is not because everyone agrees that it is the best indicator but rather because of the length of the available record. Traditionally, sunspot numbers are given as daily numbers, monthly averages, yearly averages, and smoothed numbers. The standard smoothing is a 13-month running mean centered on the month in question and using half weights for the months at the start and end. Solar cycle maxima and minima are usually given in terms of these smoothed numbers.

Additional sunspot numbers do exist. The Boulder Sunspot Number is derived from the daily Solar Region Summary produced by the US Air Force and National Oceanic and Atmospheric Administration (USAF/NOAA) from sunspot drawings obtained from the Solar Optical Observing Network (SOON) sites since 1977. These summaries identify each sunspot group and list the number of spots in each group. The Boulder Sunspot Number is then obtained using Equation (1) with $k = 1.0$. This Boulder Sunspot Number is typically about 55% larger than the International Sunspot Number (corresponding to a correction factor $k = 0.65$) but is available promptly on a daily basis while the International Sunspot Number is posted monthly. The relationship between the smoothed Boulder and International Sunspot Number is shown in Figure 3.

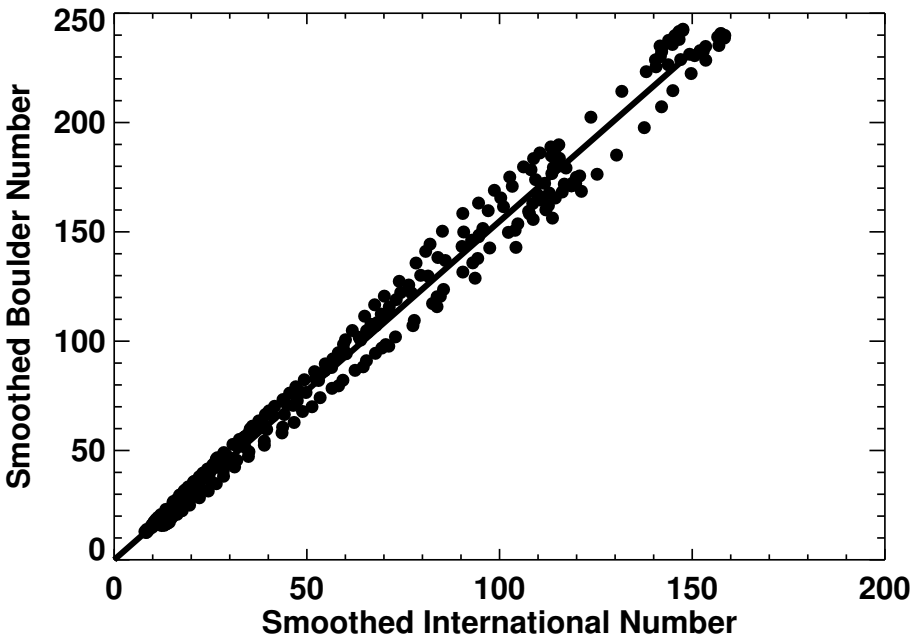

Figure 3: Boulder Sunspot Number vs. the International Sunspot Number at monthly intervals from 1981 to 2007. The average ratio of the two is 1.55 and is represented by the solid line through the data points. The Boulder Sunspot Numbers can be brought into line with the International Sunspot Numbers by using a correction factor $k = 0.65$ for Boulder.

A third sunspot number estimate is provided by the American Association of Variable Star Observers (AAVSO) and is usually referred to as the American Sunspot Number. These numbers are available from 1944 to the present. While the American Number occasionally deviates systematically from the International Number for years at a time it is usually kept closer to the International Number than the Boulder Number through its use of correction factors. (The American Number is

typically about 3% lower than the International Number.) The relationship between the American and International Sunspot number is shown in Figure 4.

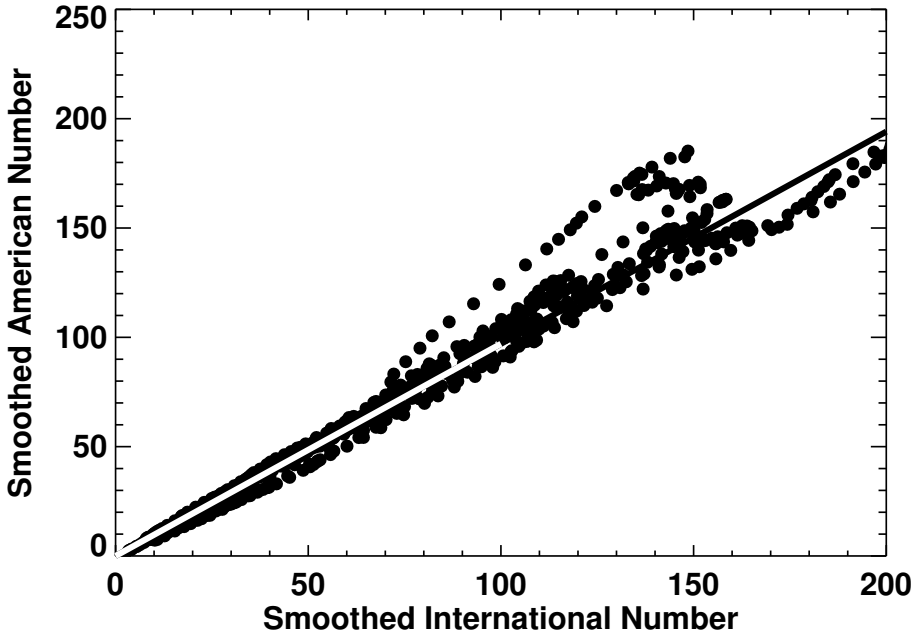

Figure 4: American Sunspot Number vs. the International Sunspot Number at monthly intervals from 1944 to 2006. The average ratio of the two is 0.97 and is represented by the solid line through the data points.

A fourth sunspot number is the Group Sunspot Number, R_G, devised by Hoyt and Schatten (1998). This index counts only the number of sunspot groups, averages together the observations from multiple observers (rather than using the primary/secondary/tertiary observer system) and normalizes the numbers to the International Sunspot Numbers using

$$R_G = \frac{12.08}{N} \sum_{i=1}^{N} k_i G_i \tag{2}$$

where N is the number of observers, k_i is the i-th observer's correction factor, G_i is the number of sunspot groups observed by observer i, and 12.08 normalizes the number to the International Sunspot Number. Hathaway *et al.* (2002) found that the Group Sunspot Number follows the International Number fairly closely but not to the extent that it should supplant the International Number. In fact, the Group Sunspot Numbers are not readily available after 1995. The primary utility of the Group Sunspot number is in extending the sunspot number observations back to the earliest telescopic observations in 1610. The relationship between the Group and International Sunspot number is shown in Figure 5 for the period 1874 to 1995. For this period the numbers agree quite well with the Group Number being about 1% higher than the International Number. For earlier dates the Group Number is a significant 24% lower than the International Number.

These sunspot numbers are available from NOAA. The International Number can be obtained monthly directly from SIDC.

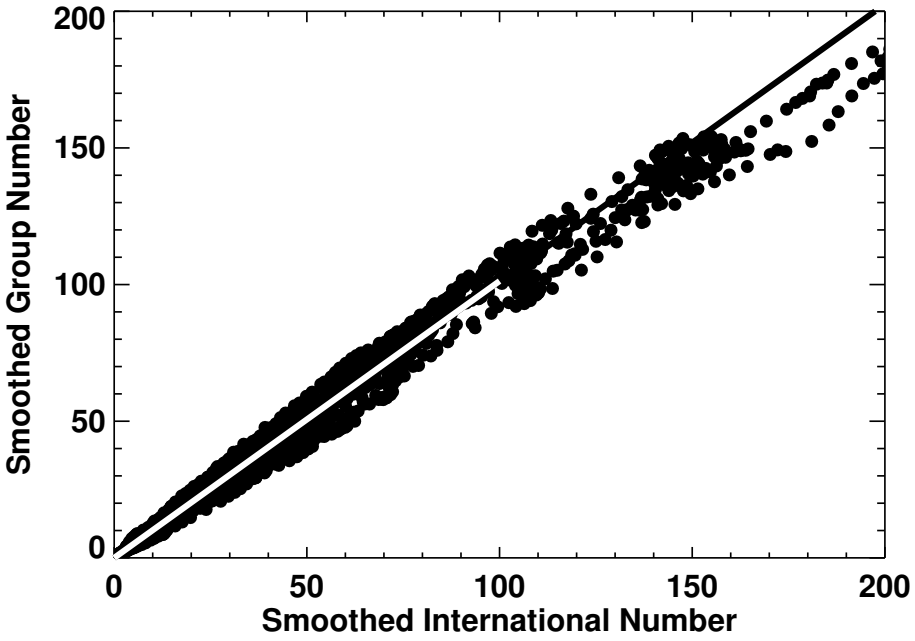

Figure 5: Group Sunspot Number vs. the International Sunspot Number at monthly intervals from 1874 to 1995. The average ratio of the two is 1.01 and is represented by the solid line through the data points.

3.2 Sunspot areas

Sunspot areas are thought to be more physical measures of solar activity. Sunspot areas and positions were diligently recorded by the Royal Observatory, Greenwich (RGO) from May of 1874 to the end of 1976 using measurements off of photographic plates obtained from RGO itself and its sister observatories in Cape Town, South Africa, Kodaikanal, India, and Mauritius. Both umbral areas and whole spot areas were measured and corrected for foreshortening on the visible disc. Sunspot areas were given in units of millionths of a solar hemisphere (μHem). Comparing the corrected whole spot areas to the International Sunspot Number (Figure 6) shows that the two quantities are indeed highly correlated ($r = 0.994$, $r^2 = 0.988$). Furthermore, there is no evidence for any lead or lag between the two quantities over each solar cycle. Both measures could almost be used interchangeably except for one aspect – the zero point. Since a single, solitary sunspot gives a sunspot number of 11 (6.6 for a correction factor $k = 0.6$) the zero point for the sunspot number is shifted slightly from zero. The best fit to the data shown in Figure 6 gives an offset of about 4 and a slope of 16.7.

In 1977 NOAA began reporting much of the same sunspot area and position information in its Solar Region Summary reports. These reports are derived from measurements taken from sunspot drawings done at the USAF SOON sites. The sunspot areas were initially estimated by overlaying a grid and counting the number of cells that a sunspot covered. In late 1981 this procedure was changed to employ an overlay with a number of circles and ellipses with different areas. The sunspot areas reported by USAF/NOAA are significantly smaller than those from RGO (Fligge and Solanki, 1997; Baranyi *et al.*, 2001; Hathaway *et al.*, 2002; Balmaceda *et al.*, 2009). Figure 7 shows the relationship between the USAF/NOAA sunspot areas and the International Sunspot Number. The slope in the straight line fit through the data is 11.32, significantly less than that found for the RGO sunspot areas. This indicates that these later sunspot area measurements should be multiplied by 1.48 to be consistent with the earlier RGO sunspot areas.

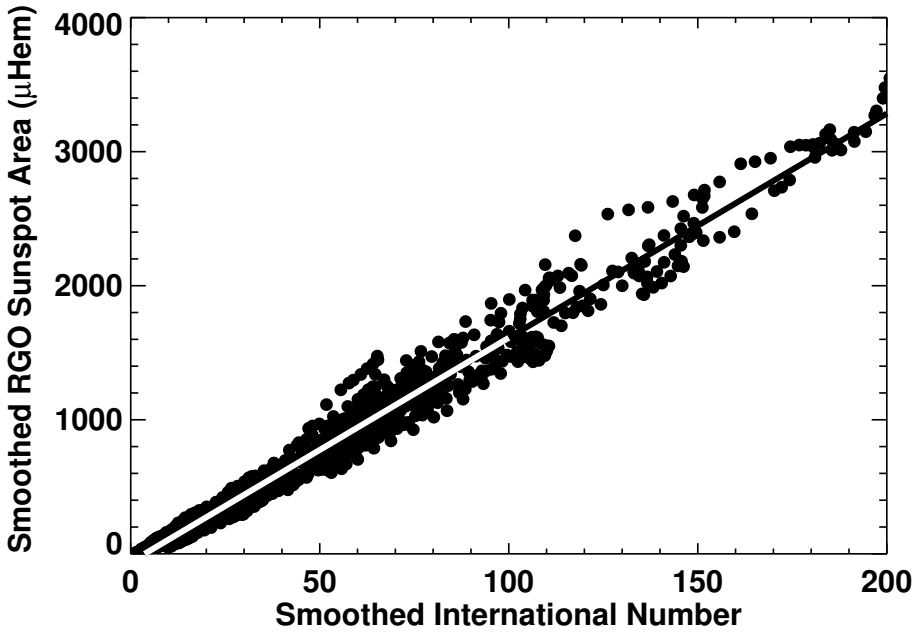

Figure 6: RGO Sunspot Area vs. the International Sunspot Number at monthly intervals from 1997 to 2010. The two quantities are correlated at the 99.4% level with a proportionality constant of about 16.7.

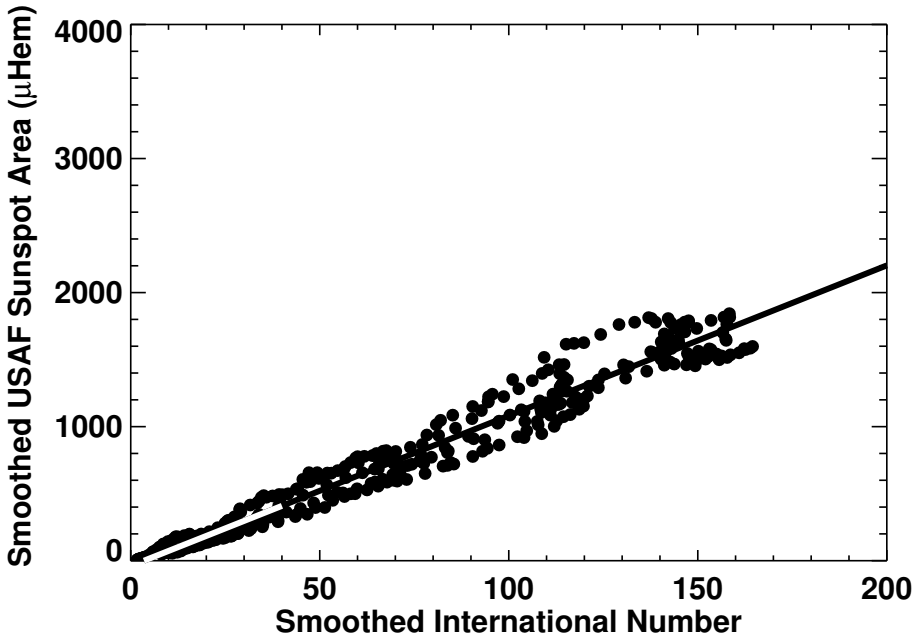

Figure 7: USAF/NOAA Sunspot Area vs. the International Sunspot Number at monthly intervals from 1977 to 2007. The two quantities are correlated at the 98.9% level with a proportionality constant of about 11.3. These sunspot areas have to be multiplied by a factor 1.48 to bring them into line with the RGO sunspot areas.

Sunspot areas are also available from a number of solar observatories including: Catania (1978 – 1999), Debrecen (1986 – 1998), Kodaikanal (1906 – 1987), Mt. Wilson (1917 – 1985), Rome (1958 – 2000), and Yunnan (1981 – 1992). While individual observatories have data gaps, their data are very useful for helping to maintain consistency over the full interval from 1874 to the present.

The combined RGO USAF/NOAA datasets are available online (RGO).

These datasets have additional information that is not reflected in sunspot numbers – positional information – both latitude and longitude. The distribution of sunspot area with latitude (Figure 8) shows that sunspots appear in two bands on either side of the Sun's equator. At the start of each cycle spots appear at latitudes above about 20 – 25°. As the cycle progresses the range of latitudes with sunspots broadens and the central latitude slowly drifts toward the equator, but with a zone of avoidance near the equator. This behavior is referred to as "Spörer's Law of Zones" by Maunder (1903) and was famously illustrated by his "Butterfly Diagram" (Maunder, 1904).

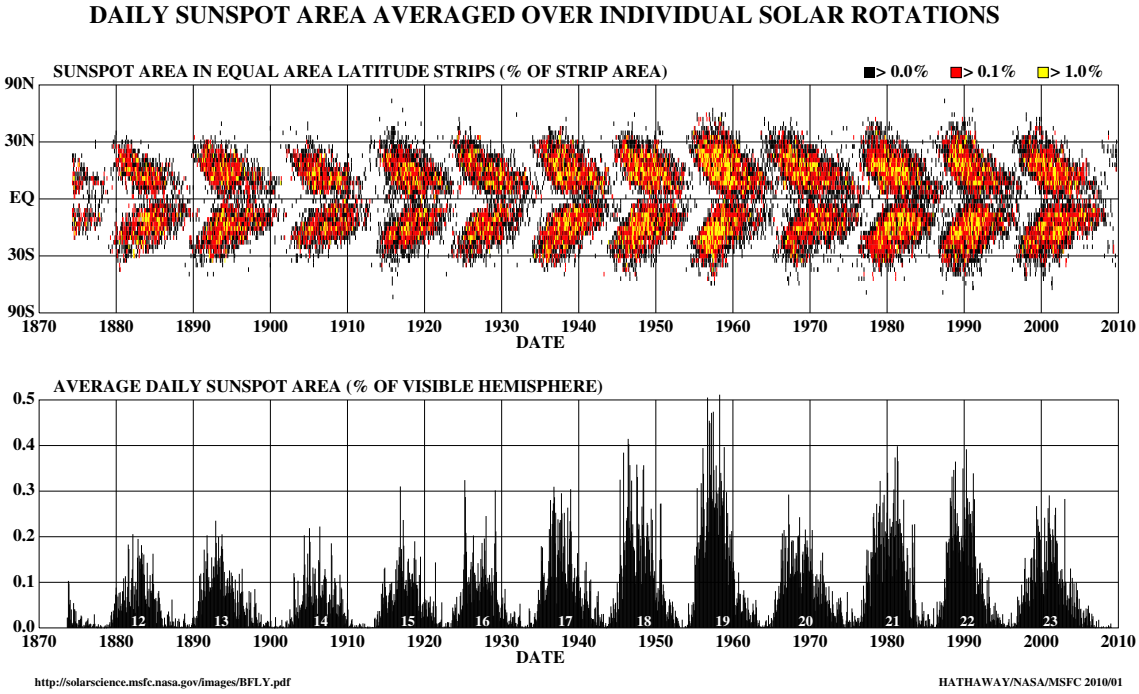

Figure 8: Sunspot area as a function of latitude and time. The average daily sunspot area for each solar rotation since May 1874 is plotted as a function of time in the lower panel. The relative area in equal area latitude strips is illustrated with a color code in the upper panel. Sunspots form in two bands, one in each hemisphere, that start at about 25° from the equator at the start of a cycle and migrate toward the equator as the cycle progresses.

3.3 10.7 cm solar flux

The 10.7 cm Solar Flux is the disk integrated emission from the Sun at the radio wavelength of 10.7 cm (2800 MHz) (cf. Tapping and Charrois, 1994). This measure of solar activity has advantages over sunspot numbers and areas in that it is completely objective and can be made under virtually all weather conditions. Measurements of this flux have been taken daily by the Canadian Solar Radio Monitoring Programme since 1946. Several measurements are taken each day and care is taken to avoid reporting values influenced by flaring activity. Observations were

made in the Ottawa area from 1946 to 1990. In 1990 a new flux monitor was installed at Penticton, British Columbia and run in parallel with the Ottawa monitor for six months before moving the Ottawa monitor itself to Penticton as a back-up. Measurements are provided daily (DRAO).

The relationship between the 10.7 cm radio flux and the International Sunspot Number is somewhat more complicated than that for sunspot area. First of all the 10.7 cm radio flux has a base level of about 67 solar flux units. Secondly, the slope of the relationship changes as the sunspot number increases up to about 30. This is captured in a formula given by Holland and Vaughn (1984) as:

$$F_{10.7} = 67 + 0.97\,R_I + 17.6\left(e^{-0.035\,R_I} - 1\right) \tag{3}$$

In addition to this slightly nonlinear relationship there is evidence that the 10.7 cm radio flux lags behind the sunspot number by about 1-month (Bachmann and White, 1994).

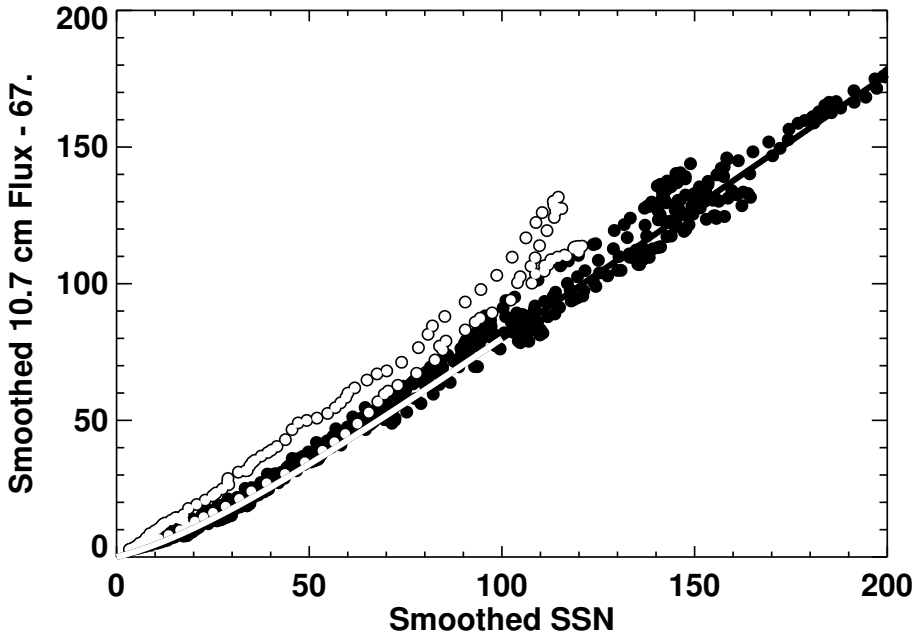

Figure 9: 10.7cm Radio Flux vs. International Sunspot Number for the period of August 1947 to March 2009. Data obtained prior to cycle 23 are shown with filled dots while data obtained during cycle 23 are shown with open circles. The Holland and Vaughn formula relating the radio flux to the sunspot number is shown with the solid line. These two quantities are correlated at the 99.7% level.

Figure 9 shows the relationship between the 10.7 cm radio flux and the International Sunspot Number. The two measures are highly correlated ($r = 0.995$, $r^2 = 0.990$). The Holland and Vaughn formula fits the early data quite well. However, the data for cycle 23 after about 1998 lies systematically higher than the levels given by the Holland and Vaughn formula.

3.4 Total irradiance

The Total Solar Irradiance (TSI) is the radiant energy emitted by the Sun at all wavelengths crossing a square meter each second outside the Earth's atmosphere. Although ground-based measurements of this "solar constant" and its variability were made decades ago (Abbot *et al.*, 1913), accurate measurements of the Sun's total irradiance have only become available with access to space. Several satellites have carried instruments designed to make these measurements: Nimbus-7 from November, 1978 to December, 1993; the Solar Maximum Mission (SMM) ACRIM-I from

February, 1980 to June, 1989; the Earth Radiation Budget Satellite (ERBS) from October, 1984 to December, 1995; NOAA-9 from January, 1985 to December, 1989; NOAA-10 from October, 1986 to April, 1987; Upper Atmosphere Research Satellite (UARS) ACRIM-II from October, 1991 to November, 2001; ACRIMSAT ACRIM-III from December, 1999 to the present; SOHO/VIRGO from January, 1996 to the present; and SORCE/TIM from January, 2003 to the present.

While each of these instruments is extremely precise in its measurements, their absolute accuracies vary in ways that make some important aspects of the TSI subjects of controversy. Figure 10 shows daily measurements of TSI from some of these instruments. Each instrument measures the drops in TSI due to the formation and disk passages of large sunspot groups as well as the general rise and fall of TSI with the sunspot cycle (Willson and Hudson, 1988). However, there are significant offsets between the absolute measured values. Intercomparisons of the data have lead to different conclusions. Willson (1997) combined the SMM/ACRIM-I data with the later UARS/ACRIM-II data by using intercomparisons with the Nimbus-7 and ERBS and concluded that the Sun was brighter by about 0.04% during the cycle 22 minimum than is was during the cycle 21 minimum. Fröhlich and Lean (1998) constructed a composite (the PMOD composite) that includes Nimbus-7, ERBS, SMM, UARS, and SOHO/VIRGO which does not show this increase.

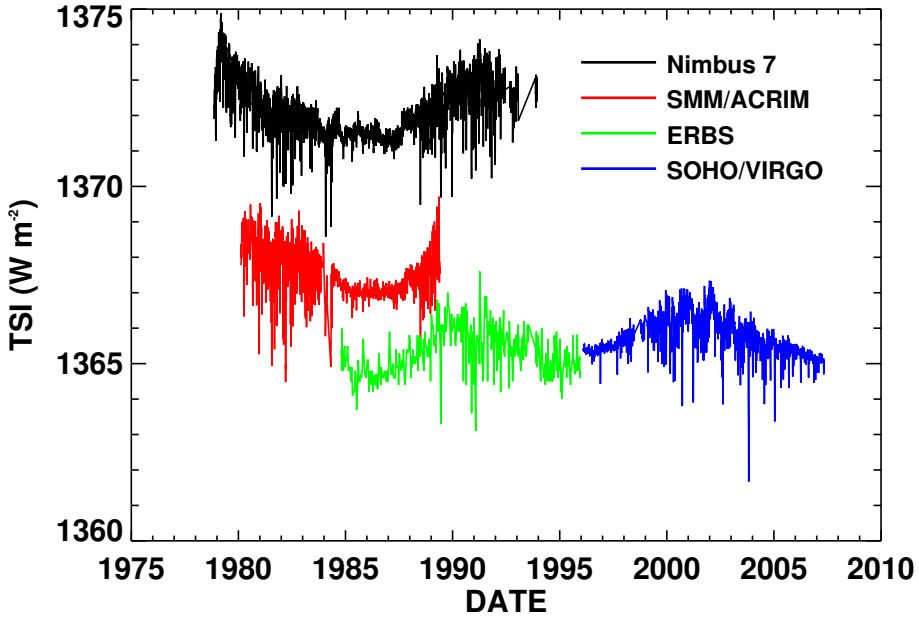

Figure 10: Daily measurements of the Total Solar Irradiance (TSI) from instruments on different satellites. The systematic offsets between measurements taken with different instruments complicate determinations of the long-term behavior.

Comparing the PMOD composite to sunspot number (Figure 11) shows a strong correlation between the two quantities but with different behavior during cycle 23. At its peak, cycle 23 had sunspot numbers about 20% smaller than cycle 21 or 22. However, the cycle 23 peak PMOD composite TSI was similar to that of cycles 21 and 22. This behavior is similar to that seen in 10.7 cm flux in Figure 9 but is complicated by the fact that the cycle 23 PMOD composite falls well below that for cycle 21 and 22 during the decline of cycle 23 toward minimum while the 10.7 cm flux remained above the corresponding levels for cycles 21 and 22.

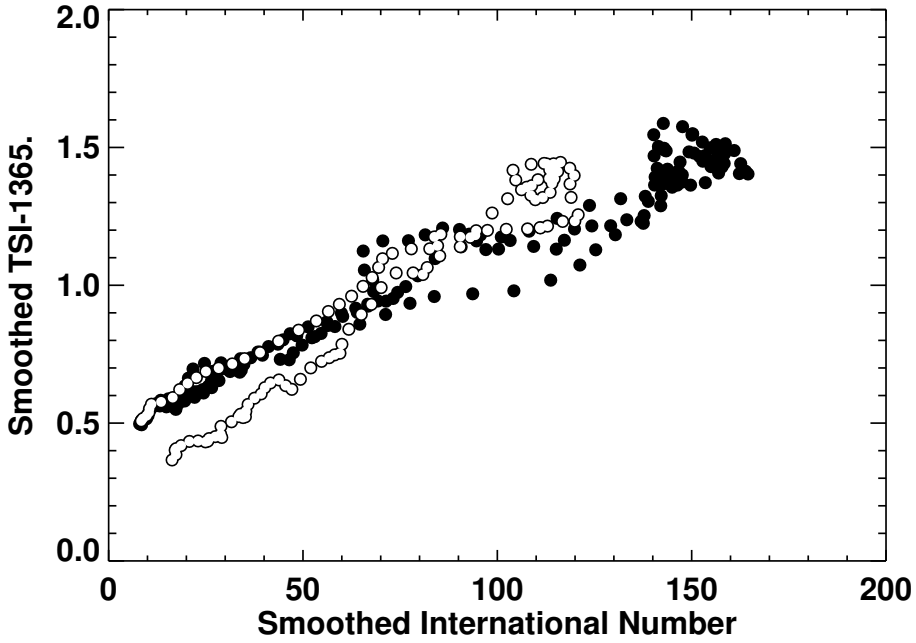

Figure 11: The PMOD composite TSI vs. International Sunspot Number. The filled circles represent smoothed monthly averages for cycles 21 and 22. The open circles represent the data for cycle 23. While the TSI at the minima preceding cycles 21 and 22 were similar in this composite, the TSI as cycle 23 approaches minimum is significantly lower. The TSI at cycle 23 maximum was similar to that in cycles 21 and 22 in spite of the fact that the sunspot number was significantly lower for cycle 23.

3.5 Magnetic field

Magnetic fields on the Sun were first measured in sunspots by Hale (1908). The magnetic nature of the solar cycle became apparent once these observations extended over more than a single cycle (Hale *et al.*, 1919). Hale *et al.* (1919) provided the first description of "Hale's Polarity Laws" for sunspots:

> "... the preceding and following spots of binary groups, with few exceptions, are of opposite polarity, and that the corresponding spots of such groups in the Northern and Southern hemispheres are also of opposite sign. Furthermore, the spots of the present cycle are opposite in polarity to those of the last cycle."

Hale's Polarity Laws are illustrated in Figure 12.

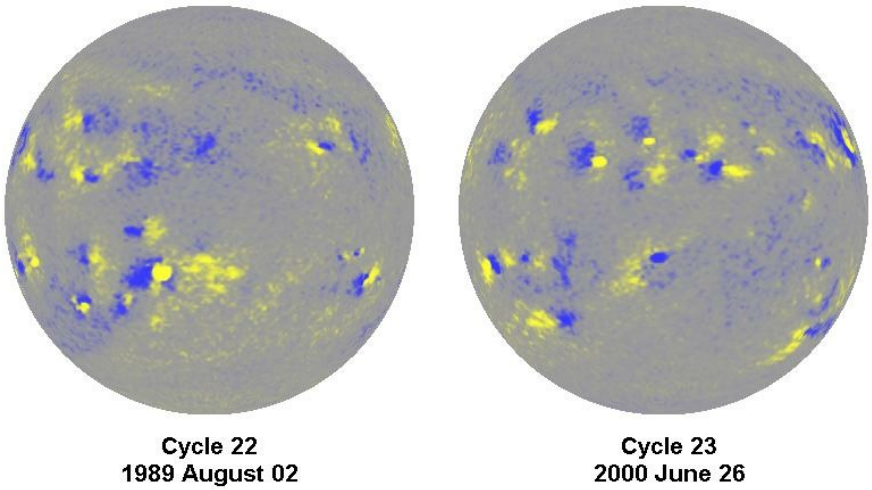

Figure 12: Hale's Polarity Laws. A magnetogram from sunspot cycle 22 (1989 August 2) is shown on the left with yellow denoting positive polarity and blue denoting negative polarity. A corresponding magnetogram from sunspot cycle 23 (2000 June 26) is shown on the right. Leading spots in one hemisphere have opposite magnetic polarity to those in the other hemisphere and the polarities flip from one cycle to the next.

In addition to Hale's Polarity Laws for sunspots, it was found that the Sun's polar fields reverse as well. Babcock (1959) noted that the polar fields reversed at about the time of sunspot cycle maximum. The Sun's south polar field reversed in mid-1957 while its north polar field reversed in late-1958. The maximum for cycle 19 occurred in late-1957. The polar fields are thus out of phase with the sunspot cycle – polar fields are at their peak near sunspot minimum. This is also indicated by the presence of polar faculae – small bright round patches seen in the polar regions in white light observations of the Sun – whose number also peak at about the time of sunspot minimum (Sheeley Jr, 1991).

Systematic, daily observations of the Sun's magnetic field over the visible solar disk were initiated at the Kitt Peak National Observatory in the early 1970s. Synoptic maps from these measurements are nearly continuous from early-1975 through mid-2003. Shortly thereafter similar (and higher resolution) data became available from the National Solar Observatory's Synoptic Optical Long-term Investigations of the Sun (SOLIS) facility (Keller, 1998). Gaps between these two datasets and within the SOLIS dataset can be filled with data from the Michelson Doppler

Imager (MDI) on the Solar and Heliospheric Observatory (SOHO) mission (Scherrer *et al.*, 1995). These synoptic maps are presented in an animation here.

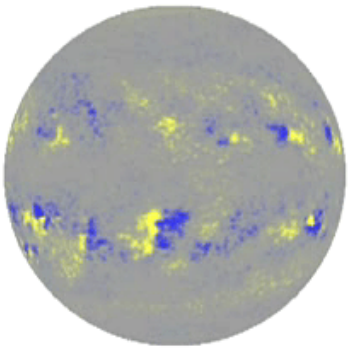

Figure 13: Still from a movie showing A full-disk magnetogram from NSO/KP used in constructing magnetic synoptic maps over the last two sunspot cycles. Yellows represent magnetic field directed outward. Blues represent magnetic field directed inward. (To watch the movie, please go to the online version of this review article at http://www.livingreviews.org/lrsp-2010-1.)

The radial magnetic field averaged over longitude for each solar rotation is shown in Figure 14. This "Magnetic Butterfly Diagram" exhibits Hale's Polarity Laws and the polar field reversals as well as "Joy's Law" (Hale *et al.*, 1919):

> "The following spot of the pair tends to appear farther from the equator than the preceding spot, and the higher the latitude, the greater is the inclination of the axis to the equator."

Joy's Law and Hale's Polarity Laws are apparent in the "butterfly wings." The equatorial sides of these wings are dominated by the lower latitude, preceding spot polarities while the poleward sides are dominated by the higher latitude (due to Joy's Law), following spot polarities. These polarities are opposite in opposite hemispheres and from one cycle to the next (Hale's Law). This figure also shows that the higher latitude fields are transported toward the poles where they eventually reverse the polar field at about the time of sunspot cycle maximum.

3.6 Flares and Coronal Mass Ejections

Carrington (1859) and Hodgson (1859) reported the first observations of a solar flare from white-light observations on September 1, 1859. While observing the Sun projected onto viewing screen Carrington noticed a brightening that lasted for about 5 minutes. Hodgson also noted a nearly simultaneous geomagnetic disturbance. Since that time flares have been observed in H-alpha from many ground-based observatories and characterizations of flares from these observations have been made (cf. Benz, 2008).

X-rays from the Sun were measured by instruments on early rocket flights and their association with solar flares was recognized immediately. NOAA has flown solar x-ray monitors on its Geostationary Operational Environmental Satellites (GOES) since 1975 as part of its Space Environment

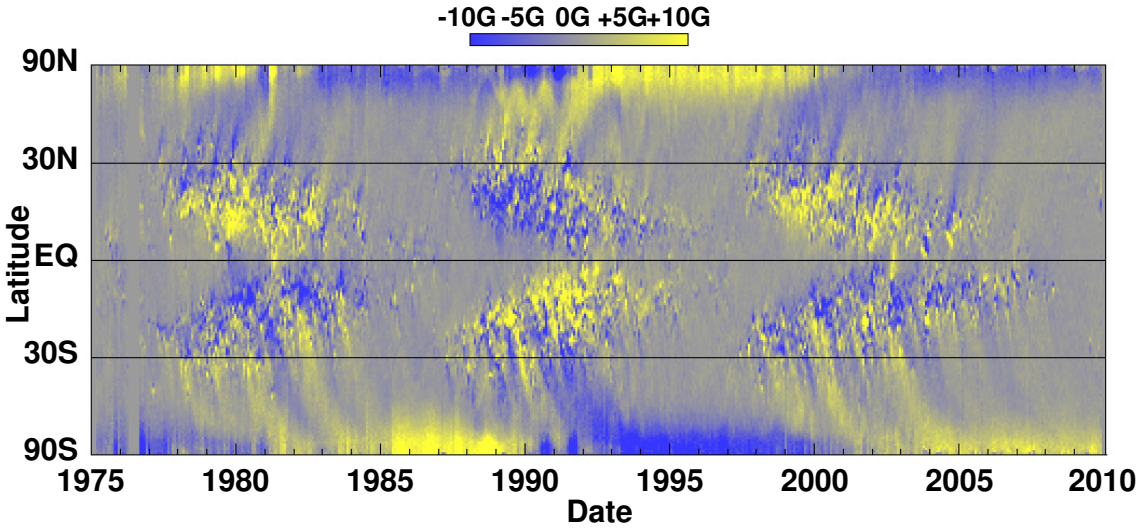

Figure 14: A Magnetic Butterfly Diagram constructed from the longitudinally averaged radial magnetic field obtained from instruments on Kitt Peak and SOHO. This illustrates Hale's Polarity Laws, Joy's Law, polar field reversals, and the transport of higher latitude magnetic field elements toward the poles.

Monitor. The solar x-ray flux has been measured in two bandpasses by these instruments: 0.5 to 4.0 Å and 1.0 to 8.0 Å. The x-ray flux is given on a logarithmic scale with A and B levels as typical background levels depending upon the phase of the cycle, and C, M, and X levels indicating increasing levels of flaring activity. The number of M-class and X-class flares seen in the 1.0 – 8.0 Å band tends to follow the sunspot number as shown in Figure 15. The two measures are well correlated ($r = 0.948$, $r^2 = 0.900$) but there is a tendency to have more flares on the declining phase of a sunspot cycle (the correlation is maximized for a 2-month lag). In spite of this correlation, significant flares can, and have, occurred at all phases of the sunspot cycle. X-class flares have occurred during the few months surrounding sunspot cycle minimum for all of the cycles observed thus far (Figure 15).

Coronal mass ejections (CMEs) are often associated with flares but can also occur in the absence of a flare. CMEs were discovered in the early 1970s from spacecraft observations from OSO 7 (Tousey, 1973) and from Skylab (MacQueen *et al.*, 1974). Routine CME observations began with the Solar Maximum Mission and continue with SOHO. The frequency of occurrence of CME's is also correlated with sunspot number (Webb and Howard, 1994).

3.7 Geomagnetic activity

Geomagnetic activity also shows a solar cycle dependence but one that is more complex than seen in sunspot area, radio flux, or flares and CMEs. There are a number of indices of geomagnetic activity, most measure rapid (hour-to-hour) changes in the strength and/or direction of the Earth's magnetic field from small networks of ground-based observatories. The *ap* index is a measure of the range of variability in the geomagnetic field (in 2 nT units) measured in three-hour intervals from a network of about 13 high latitude stations. The average of the eight daily *ap* values is given as the equivalent daily amplitude *Ap*. These indices extend from 1932 to the present. The *aa* index extends back further (to 1868 cf. Mayaud, 1972). It is similarly derived from three-hour intervals but from two antipodal stations located at latitudes of about 50°. The locations of these two stations have changed from time to time and there is evidence (Svalgaard *et al.*, 2004) that these changes are reflected in the data itself. Another frequently used index is Dst, disturbance

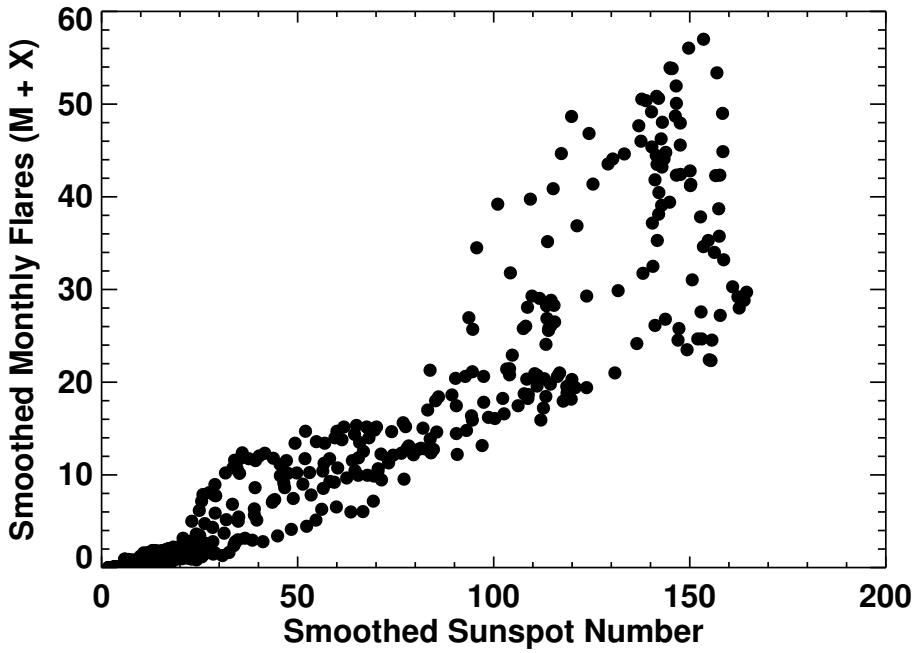

Figure 15: Monthly M- and X-class flares vs. International Sunspot Number for the period of March 1976 to January 2010. These two quantities are correlated at the 94.8% level but show significant scatter when the sunspot number is high (greater than ~ 100).

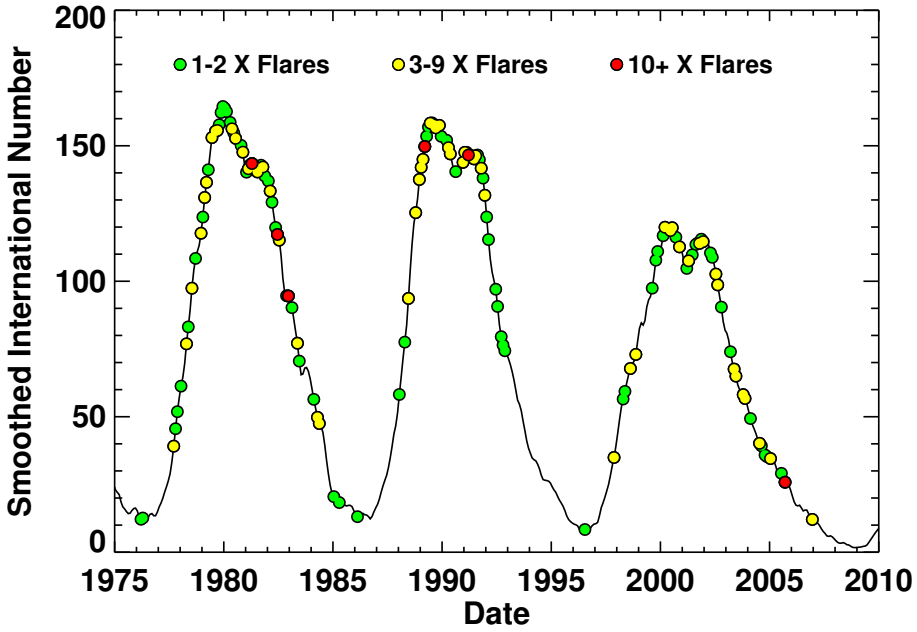

Figure 16: Monthly X-class flares and International Sunspot Number. X-class flares can occur at any phase of the sunspot cycle – including cycle minimum.

storm time, derived from measurements obtained at four equatorial stations since 1957.

Figure 17 shows the smoothed monthly geomagnetic index *aa* as a function of time along with the sunspot number for comparison. The minima in geomagnetic activity tend to occur just after those for the sunspot number and the geomagnetic activity tends to remain high during the declining phase of each cycle. This late cycle geomagnetic activity is attributed to the effects of high-speed solar wind streams from low-latitude coronal holes (cf. Legrand and Simon, 1985). Figure 17 also shows the presence of multi-cycle trends in geomagnetic activity that may be related to changes in the Sun's magnetic field (Lockwood *et al.*, 1999).

Feynman (1982) decomposed geomagnetic variability into two components – one proportional to and in phase with the sunspot cycle (the R, or Relative sunspot number component) and another out of phase with the sunspot cycle (the I, or Interplanetary component). Figure 18 shows the relationship between geomagnetic activity and sunspot number. As the sunspot number increases there is an increasing baseline level of geomagnetic activity. Feynman's R component is determined by finding this baseline level of geomagnetic activity by fitting a line proportional to Sunspot Number. The I component is then the remaining geomagnetic activity. These two components are plotted separately in Figure 19.

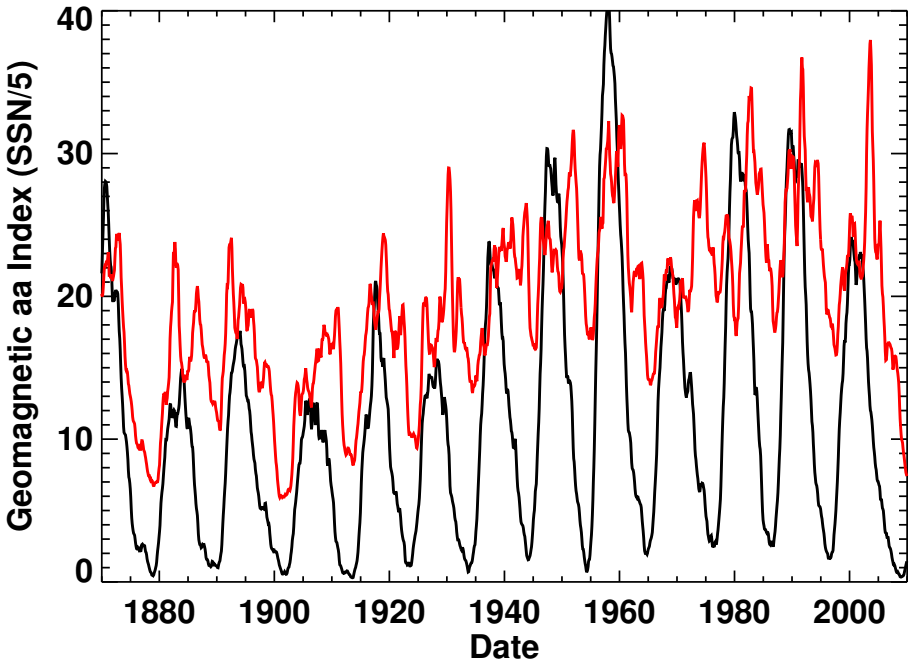

Figure 17: Geomagnetic activity and the sunspot cycle. The geomagnetic activity index aa is plotted in red. The sunspot number (divided by five) is plotted in black.

3.8 Cosmic rays

The flux of galactic cosmic rays at 1 AU is modulated by the solar cycle. Galactic cosmic rays consist of electrons and bare nuclei accelerated to GeV energies and higher at shocks produced by supernovae. The positively charged nuclei produce cascading showers of particles in the Earth's upper atmosphere that can be measured by neutron monitors at high altitude observing sites. The oldest continuously operating neutron monitor is located at Climax, Colorado, USA. Daily observations extend from 1951 to 2006. Monthly averages of the neutron counts are shown as a

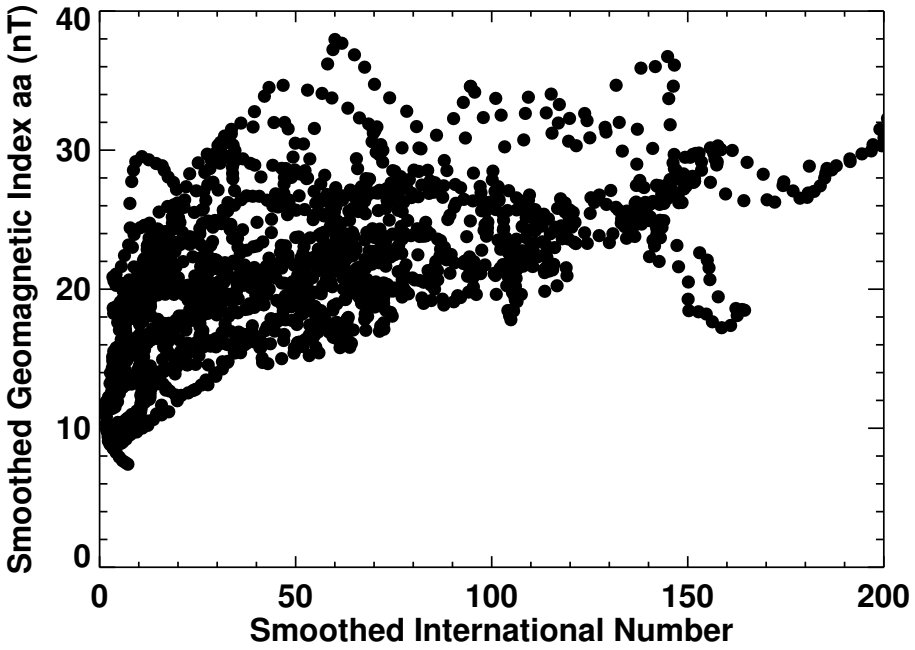

Figure 18: Geomagnetic activity index *aa* vs. Sunspot Number. As Sunspot Number increases the baseline level of geomagnetic activity increases as well.

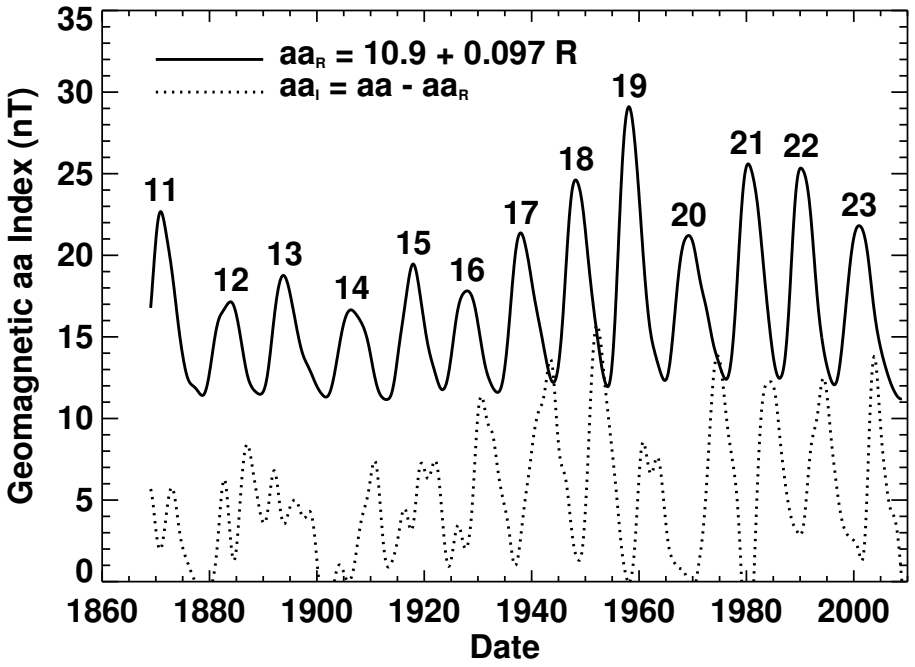

Figure 19: The smoothed R- and I-components of the geomagnetic index *aa*.

function of time in Figure 20 along with the sunspot number. As the sunspot numbers rise the neutron counts fall. This anti-correlation is attributed to scattering of the cosmic rays by tangled magnetic field within the heliosphere (Parker, 1965). At times of high solar activity magnetic structures are carried outward on the solar wind. These structures scatter cosmic rays and reduce their flux in the inner solar system.

The reduction in cosmic ray flux tends to lag behind solar activity by 6- to 12-months (Forbush, 1954) but with significant differences between the even numbered and odd numbered cycles. In the even numbered cycles (cycles 20 and 22) the cosmic ray variations seen by neutron monitors lag sunspot number variations by only about 2-months. In the odd numbered cycles (cycles 19, 21, and 23) the lag is from 10 to 14 months. Figure 20 also shows that the shapes of the cosmic ray maxima at sunspot cycle minima are different for the even and odd numbered cycles. The cosmic ray maxima (as measured by the neutron monitors) are sharply peaked at the sunspot cycle minima leading up to even numbered cycles and broadly peaked prior to odd numbered sunspot cycles. This behavior is accounted for in the transport models for galactic cosmic rays in the heliosphere (cf. Ferreira and Potgieter, 2004). The positively charged cosmic rays drift in from the heliospheric polar regions when the Sun's north polar field is directed outward (positive). When the Sun's north polar field is directed inward (negative) the positively charged cosmic rays drift inward along the heliospheric current sheet where they are scattered by corrugations in the current sheet and by magnetic clouds from CME's. The negatively charged cosmic rays (electrons) drift inward from directions (polar or equatorial) opposite to the positively charged cosmic rays that are detected by neutron monitors.

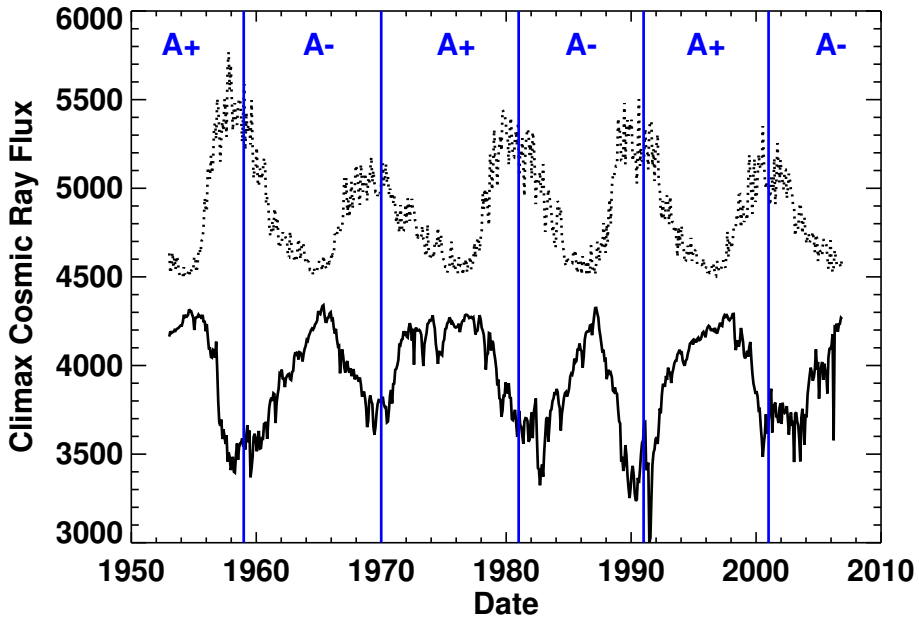

Figure 20: Cosmic Ray flux from the Climax Neutron Monitor and rescaled Sunspot Number. The monthly averaged neutron counts from the Climax Neutron Monitor are shown by the solid line. The monthly averaged sunspot numbers (multiplied by five and offset by 4500) are shown by the dotted line. Cosmic ray variations are anti-correlated with solar activity but with differences depending upon the Sun's global magnetic field polarity (A+ indicates periods with positive polarity north pole while A– indicates periods with negative polarity).

3.9 Radioisotopes in tree rings and ice cores

The radioisotopes ^{14}C and ^{10}Be are produced in the Earth's stratosphere by the impact of galactic cosmic rays on ^{14}N and ^{16}O. The ^{14}C gets oxidized to form CO_2 which is taken up by plants in general and trees in particular where it becomes fixed in annual growth rings. The ^{10}Be gets oxidized and becomes attached to aerosols that can precipitate in snow where it then becomes fixed in annual layers of ice. The solar cycle modulation of the cosmic ray flux can then lead to solar cycle related variations in the atmospheric abundances of ^{14}C (Stuiver and Quay, 1980) and ^{10}Be (Beer *et al.*, 1990). While the production rates of these two radioisotopes in the stratosphere should be anti-correlated with the sunspot cycle, the time scales involved in the transport and ultimate deposition in tree rings and ice tends to reduce and delay the solar cycle variations (cf. Masarik and Beer, 1999). Furthermore, the production rates in the stratospheric are functions of latitude and changes to the Earth's magnetic dipole moment and the latency in the stratosphere/troposphere is a function of the changing reservoirs for these chemical species. This rather complicated production/transport/storage/deposition process makes direct comparisons between Δ^{14}C (basically the difference between measured ^{14}C abundance and that expected from its 5730 year half-life) and sunspot number difficult.

4 Individual Cycle Characteristics

Each sunspot cycle has its own characteristics. Many of these characteristics are shared by other cycles and these shared characteristics provide important information for models of the solar activity cycle. A paradigm shift in sunspot cycle studies came about when Waldmeier (1935) suggested that each cycle should be treated as an individual *outburst* with its own characteristics. Prior to that time, the fashion was to consider solar activity as a superposition of Fourier components. This superposition idea probably had its roots in the work of Wolf (1859) who suggested a formula based on the orbits of Venus, Earth, Jupiter, and Saturn to fit Schwabe's data for the years 1826 to 1848.

Determining characteristics such as period and amplitude would seem simple and straight forward but the published studies show that this is not true. A prime example concerns determinations of the dates (year and month) of cycle minima. A frequently used method is to take monthly averages of the daily International Sunspot Number and to smooth these with the 13-month running mean. Unfortunately, this leaves several uncertain dates. With this method, the minimum that occurred in 1810 prior to cycle 6 could be taken as any month from April to December – all nine months had smoothed sunspot numbers of 0.0!

4.1 Minima and maxima

The dates and values for the cycle minima and maxima are the primary data for many studies of the solar cycle. These data are sensitive to the methods and input data used to find them. Solar activity is inherently noisy and it is evident that there are significant variations in solar activity on time scales shorter than 11 years (see Section 7). Waldmeier (1961) published tables of sunspot numbers along with dates and values of minima and maxima for cycles 1 to 19. McKinnon (1987) extended the data to include cycles 20 and 21. The values they give for sunspot number maxima and minima are those found using the 13-month running mean. However, the dates given for maxima and minima may vary after considering additional indicators. According to McKinnon:

> "... maximum is based in part on an average of the times extremes are reached in the monthly mean sunspot number, the smoothed monthly mean sunspot number, and in the monthly mean number of spot groups alone."

These dates and the values for sunspot cycle maxima are given in Table 1 (the number of groups is multiplied by 12.08 to produce group sunspot numbers that are comparable to the relative sunspot numbers). It is clear from this table that considerably more weight is given to the date provided by the 13-month running mean. The dates provided by Waldmeier and McKinnon are far closer to those given by the 13-month running mean than they are to the average date of the three indicators. (One exception is the date they give for the maximum of cycle 14 which should be half a year earlier by almost any averaging scheme.) The monthly numbers of sunspots and spot groups vary widely and, in fact, should be less reliable indicators and given lesser weight in determining maximum.

The minima in these three indicators have been used along with additional sunspot indicators to determine the dates of minima. The number of spotless days in a month tends to maximize at the time of minimum and the number of new cycle sunspot groups begins to exceed the number of old cycle sunspot groups at the time of minimum. Both Waldmeier and McKinnon suggest using these indicators as well when setting the dates for minima. These dates are given in Table 2 where both the spotless days per month and the number of old cycle and new cycle groups per month are smoothed with the same 13-month mean filter. The average date given in the last column is the average of the 13-month mean minimum date, the 13-month mean spotless days per month maximum date, and the date when the 13-month mean of the number of new cycle groups exceeds

Table 1: Dates and values for sunspot cycle maxima.

Cycle	Waldmeier/ McKinnon		13-month Mean Maximum		Monthly Mean Maximum		Monthly Group Maximum	
	Date	Value	Date	Value	Date	Value	Date	Value
1	1761.5	86.5	1761/06	86.5	1761/05	107.2	1761/05	109.4
2	1769.7	115.8	1769/09	115.8	1769/10	158.2	1771/05	162.5
3	1778.4	158.5	1778/05	158.5	1778/05	238.9	1778/01	144.0
4	1788.1	141.2	1788/02	141.2	1787/12	174.0	1787/12	169.0
5	1805.2	49.2	1805/02	49.2	1804/10	62.3	1805/11	67.0
6	1816.4	48.7	1816/05	48.7	1817/03	96.2	1817/03	57.0
7	1829.9	71.7	1829/11	71.5	1830/04	106.3	1830/04	101.5
8	1837.2	146.9	1837/03	146.9	1836/12	206.2	1837/01	160.7
9	1848.1	131.6	1848/02	131.9	1847/10	180.4	1849/01	130.9
10	1860.1	97.9	1860/02	98.0	1860/07	116.7	1860/07	103.4
11	1870.6	140.5	1870/08	140.3	1870/05	176.0	1870/05	122.3
12	1883.9	74.6	1883/12	74.6	1882/04	95.8	1884/01	86.0
13	1894.1	87.9	1894/01	87.9	1893/08	129.2	1893/08	126.7
14	1907.0?	64.2	1906/02	64.2	1907/02	108.2	1906/07	111.6
15	1917.6	105.4	1917/08	105.4	1917/08	154.5	1917/08	157.0
16	1928.4	78.1	1928/04	78.1	1929/12	108.0	1929/12	121.8
17	1937.4	119.2	1937/04	119.2	1938/07	165.3	1937/02	154.5
18	1947.5	151.8	1947/05	151.8	1947/05	201.3	1947/07	149.3
19	1957.9	201.3	1958/03	201.3	1957/10	253.8	1957/10	222.2
20	1968.9	110.6	1968/11	110.6	1969/03	135.8	1968/05	132.3
21	1979.9	164.5	1979/12	164.5	1979/09	188.4	1979/01	179.4
22			1989/07	158.5	1990/08	200.3	1990/08	195.9
23			2000/04	120.7	2000/07	169.1	2000/07	153.9

the 13-month mean of the number of old cycle groups. For the early cycles, where spotless days and old and new cycle groups are not available, the 13-month mean minimum date is used for those dates in forming the average.

Table 2: Dates and values for sunspot cycle minima. The value is always the value of the 13-month mean of the International sunspot number. The dates differ according to the indicator used.

Cycle	13-month Mean Minimum		Waldmeier/ McKinnon	Spotless Days Maximum	New > Old	Average
	Date	Value	Date	Date	Date	Date
1	1755/02	8.4	1755.2			1755/02
2	1766/06	11.2	1766.5			1766/06
3	1775/06	7.2	1775.5			1775/06
4	1784/09	9.5	1784.7			1784/09
5	1798/04	3.2	1798.3			1798/04
6	1810/08	0.0	1810.6			1810/08
7	1823/05	0.1	1823.3	1823/02		1823/04
8	1833/11	7.3	1833.9	1833/11		1833/11
9	1843/07	10.6	1843.5	1843/07		1843/07
10	1855/12	3.2	1856.0	1855/12		1855/12
11	1867/03	5.2	1867.2	1867/05		1867/04
12	1878/12	2.2	1878.9	1878/10	1879/01	1878/12
13	1890/03	5.0	1889.6	1890/02	1889/09	1890/01
14	1902/01	2.7	1901.7	1902/01	1901/11	1901/12
15	1913/07	1.5	1913.6	1913/08	1913/04	1913/06
16	1923/08	5.6	1923.6	1923/10	1923/09	1923/09
17	1933/09	3.5	1933.8	1933/09	1933/11	1933/10
18	1944/02	7.7	1944.2	1944/02	1944/03	1944/02
19	1954/04	3.4	1954.3	1954/04	1954/04	1954/04
20	1964/10	9.6	1964.9	1964/11	1964/08	1964/10
21	1976/03	12.2	1976.5	1975/09	1976/08	1976/03
22	1986/09	12.3		1986/03	1986/10	1986/07
23	1996/05	8.0		1996/07	1996/12	1996/08
24	2008/12	1.7		2008/12	2008/09	2008/11

When available, all three indicators tend to give dates that are fairly close to each other and the average of the three is usually close to the dates provided by Waldmeier and McKinnon. There are, however, two notable exceptions. The dates given by Waldmeier for the minima preceding cycles 13 and 14 are both significantly earlier than the dates given by all three indicators. The cycle 13 minimum date of 1889.6 was adopted from Wolf (1892) while the cycle 14 minimum date of 1901.7 was adopted from Wolfer (1903).

Since many researchers simply adopt the date given by the minimum in the 13-month running mean, the date for the minimum preceding cycle 23 is also problematic. The minimum in smoothed sunspot number came in May of 1996. The maximum in the smoothed number of spotless days per month came in July of 1996. However, the cross-over in the smoothed number of groups from old-cycle to new cycle occurred in December of 1996. Harvey and White (1999) provide a good discussion of the problems in determining cycle minimum and have argued that the minimum for cycle 23 should be taken as September 1996 (based on their determination that new cycle groups exceed old cycle groups in January of 1997). The average of the three indicators gives August of 1996.

Additional problems in assigning dates and values to maxima and minima can be seen when using data other than sunspot numbers. Table 3 lists the dates and values for cycle maxima using the 13-month running mean on sunspot numbers, sunspot areas, and 10.7 cm radio flux. The sunspot areas have been converted to sunspot number equivalents using the relationship shown in Figure 6 and the 10.7 cm radio flux has been converted into sunspot number equivalents using Equation (3). Very significant differences can be seen in the dates. Over the last five cycles the ranges in dates given by the different indices have been: 4, 27, 25, 1, and 22 months.

Table 3: Dates and values of maxima using the 13-month running mean with sunspot number data, sunspot area data, and 10.7 cm radio flux data.

Cycle	13-month Mean Maximum		13-month Mean Sunspot Area		13-month Mean 10.7 cm Flux	
	Date	Value	Date	R-Value	Date	R-Value
1	1761/06	86.5				
2	1769/09	115.8				
3	1778/05	158.5				
4	1788/02	141.2				
5	1805/02	49.2				
6	1816/05	48.7				
7	1829/11	71.5				
8	1837/03	146.9				
9	1848/02	131.9				
10	1860/02	98.0				
11	1870/08	140.3				
12	1883/12	74.6	1883/11	88.3		
13	1894/01	87.9	1894/01	100.4		
14	1906/02	64.2	1905/06	75.4		
15	1917/08	105.4	1917/08	93.0		
16	1928/04	78.1	1926/04	92.3		
17	1937/04	119.2	1937/05	133.3		
18	1947/05	151.8	1947/05	166.5		
19	1958/03	201.3	1957/11	216.5	1958/03	201.2
20	1968/11	110.6	1968/04	100.9	1970/07	109.6
21	1979/12	164.5	1982/01	156.0	1981/05	159.4
22	1989/07	158.5	1989/06	158.5	1989/06	168.0
23	2000/04	120.7	2002/02	126.7	2002/02	152.3

These tables illustrate the problems in determining dates and values for cycle minima and maxima. The crux of the problem is in the short-term variability of solar activity. One solution is to use different smoothing.

4.2 Smoothing

The monthly averages of the daily International Sunspot Number are noisy and must be smoothed in some manner in order to determine appropriate values for parameters such as minima, maxima, and their dates of occurrence. The daily values themselves are relatively uncertain. They depend upon the number and the quality of observations as well as the time of day when they are taken (the sunspot number changes over the course of the day as spots form and fade away). The monthly averages of these daily values are also problematic. The Sun rotates once in about 27-days but the

months vary in length from 28 to 31 days. If the Sun is particularly active at one set of longitudes then some monthly averages will include one appearance of these active longitudes while other months will include two. This aspect is particularly important for investigations of short-term (months) variability (see Section 7). For long-term (years) variability this can be treated as noise and filtered out.

The traditional 13-month running mean (centered on a given month with equal weights for months –5 to +5 and half weight for months –6 and +6) is both simple and widely used but does a poor job of filtering out high frequency variations (although it is better than the simple 12-month average). Gaussian shaped filters are preferable because they have Gaussian shapes in the frequency domain and effectively remove high frequency variations (Hathaway *et al.*, 1999). A tapered (to make the filter weights and their first derivatives vanish at the end points) Gaussian filter is given by

$$W(t) = e^{-t^2/2a^2} - e^{-2}\left(3 - t^2/2a^2\right) \tag{4}$$

with

$$-2a + 1 \leq t \leq +2a - 1 \tag{5}$$

where t is the time in months and $2a$ is the FWHM of the filter (note that this formula is slightly different than that given in Hathaway *et al.* (1999). There are significant variations in solar activity on time scales of one to three years (see Section 7). These variations can produce double peaked maxima which are filtered out by a 24-month Gaussian filter. The frequency responses of these filters are shown in Figure 21.

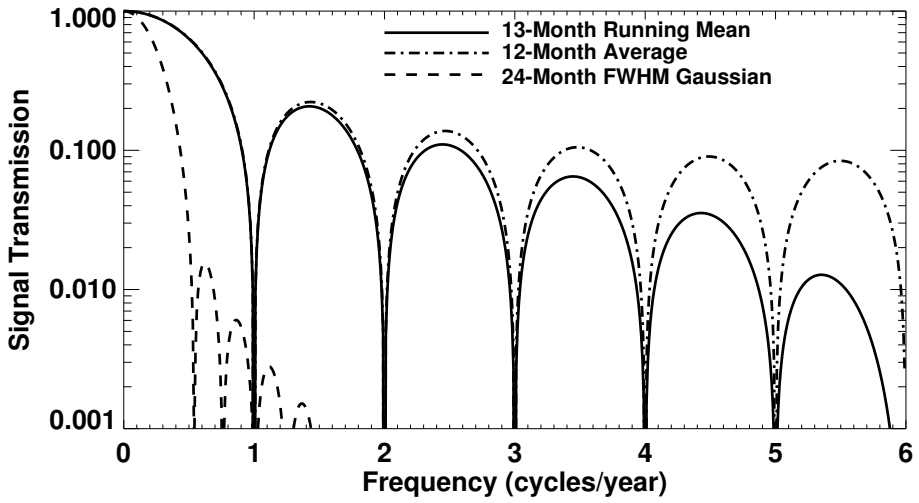

Figure 21: Signal transmission for filters used to smooth monthly sunspot numbers. The 13-month running mean and the 12-month average pass significant fractions (as much as 20%) of signals with frequencies higher than 1/year. The 24-month FWHM Gaussian passes less than 0.3% of those frequencies and passes less than about 1% of the signal with frequencies of 1/2-years or higher.

Using the 24-month FWHM Gaussian filter on the data used to create Table 3 gives far more consistent results for both maxima and minima. The results for maxima are shown in Table 4. The ranges of dates for the last five maxima become: 1, 10, 13, 4, and 11 months – roughly half the ranges found using the 13-month running mean.

Table 4: Dates and values of maxima using the 24-month FWHM Gaussian with sunspot number data, sunspot area data, and 10.7 cm radio flux data as in Table 3.

Cycle	24-month Gaussian Maximum		24-Month Gaussian Sunspot Area		24-Month Gaussian 10.7 cm Flux	
	Date	Value	Date	R-Value	Date	R-Value
1	1761/05	72.9				
2	1770/01	100.5				
3	1778/09	137.4				
4	1788/03	130.6				
5	1804/06	45.7				
6	1816/08	43.8				
7	1829/10	67.1				
8	1837/04	146.9				
9	1848/06	115.7				
10	1860/03	92.1				
11	1870/11	138.5				
12	1883/11	64.7	1883/10	70.8		
13	1893/09	81.4	1893/09	84.7		
14	1906/05	59.6	1906/04	62.4		
15	1917/12	88.6	1918/01	79.6		
16	1927/12	71.6	1926/12	75.9		
17	1937/11	108.2	1938/02	118.1		
18	1948/03	141.7	1947/09	140.0		
19	1958/02	188.0	1958/03	192.0	1958/03	188.1
20	1969/03	106.6	1968/09	95.5	1969/07	104.6
21	1980/05	151.8	1981/06	140.2	1980/11	153.1
22	1990/02	149.2	1990/06	141.7	1990/06	156.1
23	2000/12	112.7	2001/11	106.2	2001/06	136.4

4.3 Cycle periods

The period of a sunspot cycle is defined as the elapsed time from the minimum preceding its maximum to the minimum following its maximum. This does not, of course, account for the fact that each cycle actually starts well before its preceding minimum and continues long after its following minimum. By this definition, a cycle's period is dependent upon the behavior of both the preceding and following cycles. The measured period of a cycle is also subject to the uncertainties in determining the dates of minimum as indicated in the previous subsections. Nonetheless, the length of a sunspot cycle is a key characteristic and variations in cycle periods have been well studied. The average cycle period can be fairly accurately determined by simply subtracting the date for the minimum preceding cycle 1 from the date for the minimum preceding cycle 23 and dividing by the 22 cycles those dates encompass. This gives an average period for cycles 1 to 22 of 131.7 months – almost exactly 11 years.

The distribution of cycle periods depends upon the cycles used and the methods used to determine minima. Eddy (1977) noted that the cycle periods did not appear to be distributed normally. Wilson (1987) included cycle 8 to 20 and used the dates for minimum from the 13-month mean of the monthly sunspot numbers and found that a bimodal distribution best fit the data with short period (122 month) cycles and long period (140 month) cycles separated by a gap (the Wilson Gap) surrounding the mean cycle length of 132.8 months. However, Hathaway *et al.* (2002) used minima dates from the 24-month Gaussian smoothing of the International Sunspot number for cycles 1 to 23 and of the Group Sunspot Numbers for cycles –4 to 23 and found distributions that were consistent with a normal distributions about a mean of 131 months with a standard deviation of 14 months and no evidence of a gap. These cycle periods and their distributions are shown in Figure 22.

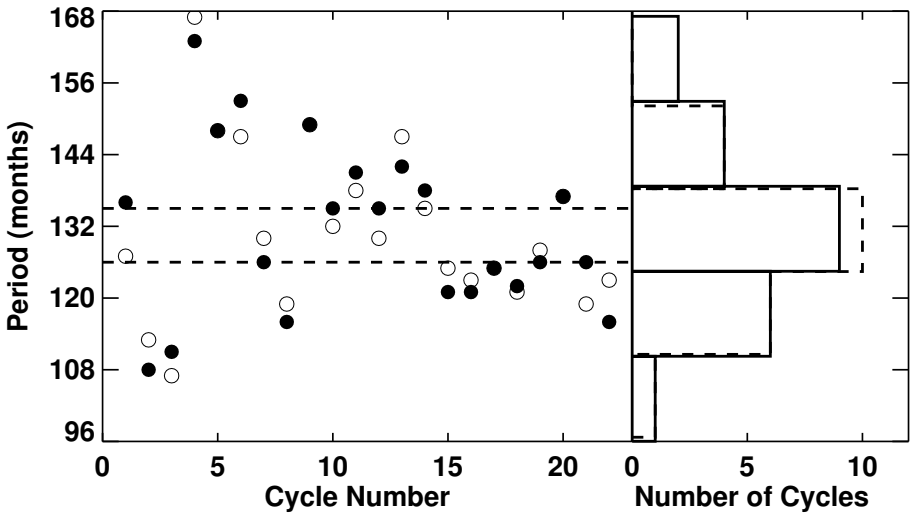

Figure 22: The left panel shows cycle periods as functions of Cycle Number. Filled circles give periods determined from minima in the 13-month mean while open circles give periods determined from the 24-month Gaussian smoothing. Both measurements give a mean period of about 131 months with a standard deviation of about 14 months. The "Wilson Gap" in periods between 125 and 134 months from the 13-month mean is shown with the dashed lines. The right panel shows histograms of cycle periods centered on the mean period with bin widths of one standard deviation. The solid lines show the distribution from the 13-month mean while the dashed lines show the distribution for the 24-month Gaussian. The periods appear normally distributed and the "Wilson Gap" is well populated with the 24-month Gaussian smoothed data.

4.4 Cycle amplitudes

The amplitude of a cycle is another key characteristic. As we have seen in Tables 3 and 4, the actual value for the amplitude of a cycle depends upon the activity index used and the type of smoothing. These uncertainties can even change the relative amplitudes of the cycles. In Table 3 we see that the second largest cycle is cycle 21 according to the 13-month mean of the International Sunspot Numbers but with the same smoothing the second largest in sunspot area and 10.7 cm flux is cycle 22. Cycles 15 and 16 were very similar according to sunspot area but cycle 15 is significantly larger than cycle 16 according to the International Sunspot Number. The Group Sunspot Numbers do provide information on earlier cycles but show systematic differences when compared to the International Sunspot Numbers. The maxima determined by the 13-month mean with the International Sunspot Numbers and the Group Sunspot Numbers are given in Table 5.

Table 5: Cycle maxima determined by the 13-month mean with the International Sunspot Numbers and the Group Sunspot Numbers. The Group values are systematically lower than the International values prior to cycle 12.

Cycle	International Maximum		Group SSN Maximum	
	Date	Value	Date	Value
–4			1705/05	5.5
–3			1719/11	34.2
–2			1730/02	82.6
–1			1739/05	58.3
0			1750/03	70.6
1	1761/06	86.5	1761/05	71.3
2	1769/09	115.8	1769/09	106.5
3	1778/05	158.5	1779/06	79.5
4	1788/02	141.2	1787/10	90.5
5	1805/02	49.2	1805/06	24.8
6	1816/05	48.7	1816/09	31.5
7	1829/11	71.5	1829/12	64.4
8	1837/03	146.9	1837/03	116.8
9	1848/02	131.9	1848/11	93.2
10	1860/02	98.0	1860/10	85.8
11	1870/08	140.3	1870/11	99.9
12	1883/12	74.6	1884/03	68.2
13	1894/01	87.9	1894/01	96.0
14	1906/02	64.2	1906/02	64.6
15	1917/08	105.4	1917/08	111.3
16	1928/04	78.1	1928/07	81.6
17	1937/04	119.2	1937/04	125.1
18	1947/05	151.8	1947/07	145.2
19	1958/03	201.3	1958/03	186.1
20	1968/11	110.6	1970/06	109.3
21	1979/12	164.5	1979/07	154.2
22	1989/07	158.5	1991/02	153.5
23	2000/04	120.7	2001/12	123.6

These cycle maxima and their distributions are shown in Figure 23. The mean amplitude of

cycles 1 to 23 from the International Sunspot Numbers is 114 with a standard deviation of 40. The mean amplitude of Cycles –4 to 23 from the Group Sunspot Numbers is 90 with a standard deviation of 41.

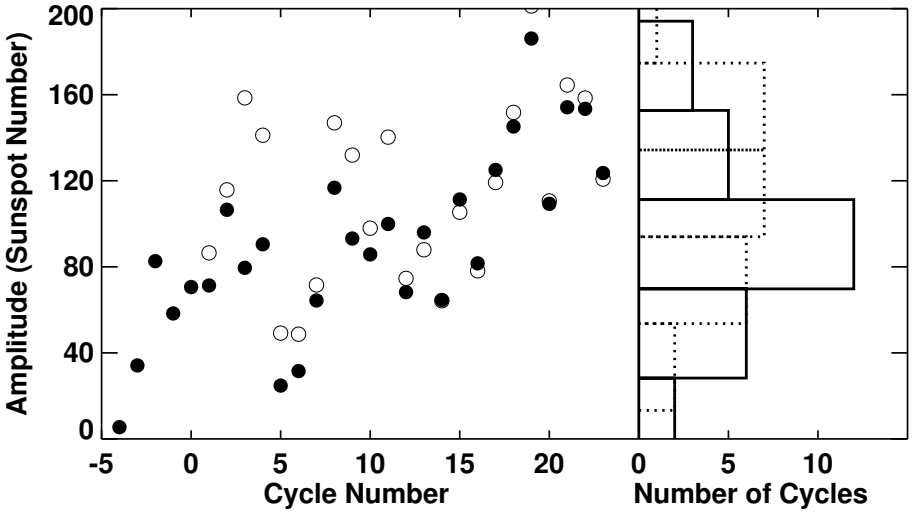

Figure 23: The left panel shows cycle amplitudes as functions of cycle number. The filled circles show the 13-month mean maxima with the Group Sunspot Numbers while the open circles show the maxima with the International Sunspot Numbers. The right panel shows the cycle amplitude distributions (solid lines for the Group values, dotted lines for the International values). The Group amplitudes are systematically lower than the International amplitudes for cycles prior to cycle 12 and have a nearly normal distribution. The amplitudes for the International Sunspot Number are skewed toward higher values.

4.5 Cycle shape

Sunspot cycles are asymmetric with respect to their maxima (Waldmeier, 1935). The elapsed time from minimum up to maximum is almost always shorter than the elapsed time from maximum down to minimum. An average cycle can be constructed by stretching and contracting each cycle to the average length, normalizing each to the average amplitude, and then taking the average at each month. This is shown in Figure 24 for cycles 1 to 22. The average cycle takes about 48 months to rise from minimum up to maximum and about 84 months to fall back to minimum again.

Various functions have been used to fit the shape of the cycle and/or its various phases. Stewart and Panofsky (1938) proposed a single function for the full cycle that was the product of a power law for the initial rise and an exponential for the decline. They found the four parameters (starting time, amplitude, exponent for the rise, and time constant for the decline) that give the best fit for each cycle. Nordemann (1992) fit both the rise and the decay with exponentials that each required three parameters – an amplitude, a time constant, and a starting time. Elling and Schwentek (1992) also fit the full cycle but with a modified F-distribution density function which requires five parameters. Hathaway *et al.* (1994) suggested yet another function – similar to that of Stewart and Panofsky (1938) but with a fixed (cubic) power law and a Gaussian for the decline. This function of time

$$F(t) = A \left(\frac{t - t_0}{b} \right)^3 \left[\exp \left(\frac{t - t_0}{b} \right)^2 - c \right]^{-1} \tag{6}$$

has four parameters: an amplitude A, a starting time t_0, a rise time b, and an asymmetry parameter c. The average cycle is well fit with $A = 193$, $b = 54$, $c = 0.8$, and $t_0 = 4$ months prior to minimum.

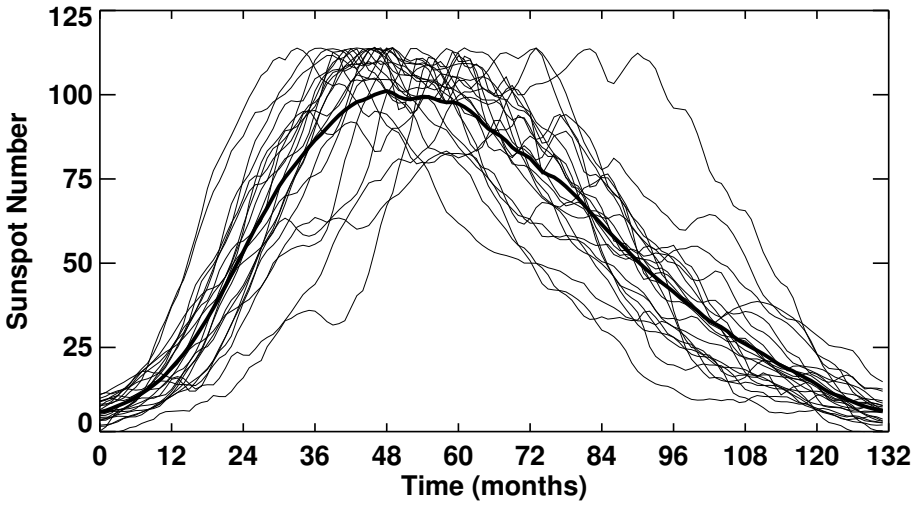

Figure 24: The average of cycles 1 to 22 (thick line) normalized to the average amplitude and period. The average cycle is asymmetric in time with a rise to maximum over 4 years and a fall back to minimum over 7 years. The 22 individual, normalized cycles are shown with the thin lines.

This fit to the average cycle is shown in Figure 25. Hathaway *et al.* (1994) found that good fits to most cycles could be obtained with a fixed value for the parameter c and a parameter b that is allowed to vary with the amplitude – leaving a function of just two parameters – amplitude and starting time.

4.6 Rise time vs. amplitude (The Waldmeier Effect)

A number of relationships have been found between various sunspot cycle characteristics. Among the more significant relationships is the Waldmeier Effect (Waldmeier, 1935, 1939) in which the time it takes for the sunspot number to rise from minimum to maximum is inversely proportional to the cycle amplitude. This is shown in Figure 26 for both the International Sunspot Number and the 10.7 cm radio flux data. Times and values for the maxima are taken from the 24-month Gaussian given in Table 4. Times for the minima are taken from the average dates given in Table 2. Both of these indices exhibit the Waldmeier Effect but with the 10.7 cm flux maxima delayed by about 6 months. This is larger than, but consistent with the delays seen by Bachmann and White (1994). The best fit through the Sunspot Number data gives

$$\text{Rise Time (in months)} \approx 35 + 1800/\text{Amplitude (in Sunspot Number)}. \quad (7)$$

While this effect is widely quoted and accepted it does face a number of problems. Hathaway *et al.* (2002) found that the effect was greatly diminished when Group Sunspot Numbers were used (the anti-correlation between rise time and amplitude dropped from –0.7 to –0.34). Inspection of Figure 26 clearly shows significant scatter. Dikpati *et al.* (2008b) noted that the effect is not seen for sunspot area data. This is consistent with the date in Tables 3 and 4 which show that significantly different dates for maxima are found with sunspot area when compared to sunspot number. The dates can differ by more than a year but without any evidence of systematic differences (area sometimes leads number and other times lags).

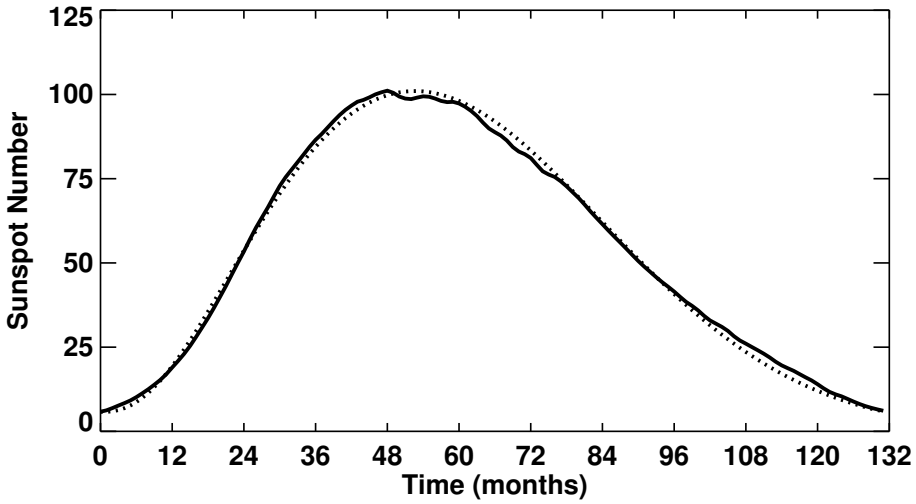

Figure 25: The average cycle (solid line) and the Hathaway *et al.* (1994) functional fit to it (dotted line) from Equation (6). This fit has the average cycle starting 4 months prior to minimum, rising to maximum over the next 54 months, and continuing about 18 months into the next cycle.

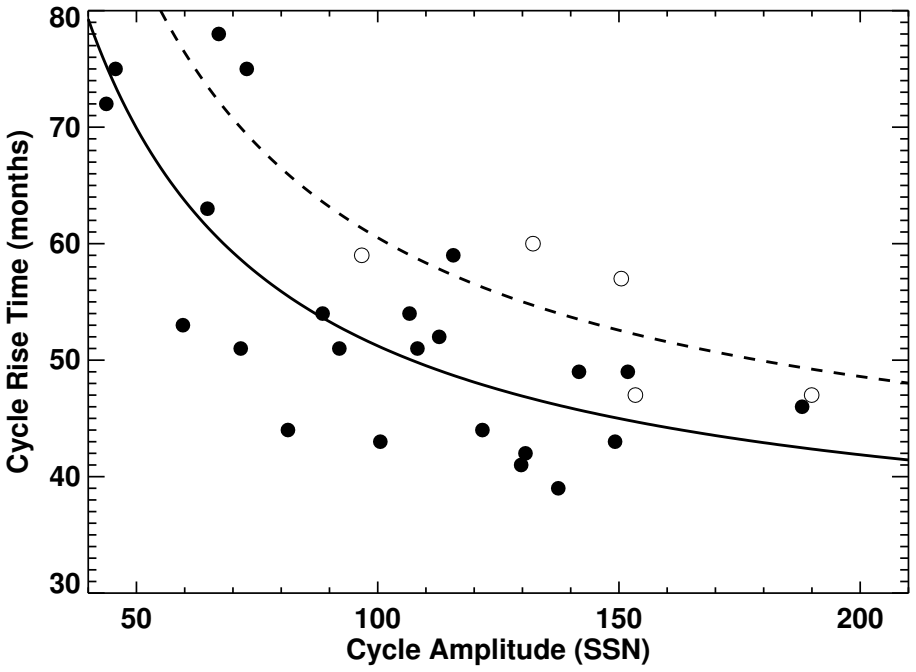

Figure 26: The Waldmeier Effect. The cycle rise time (from minimum to maximum) plotted versus cycle amplitude for International Sunspot Number data from cycles 1 to 23 (filled dots) and for 10.7 cm Radio Flux data from cycles 19 to 23 (open circles). This gives an inverse relationship between amplitude and rise time shown by the solid line for the Sunspot Number data and with the dashed line for the Radio Flux data. The Radio Flux maxima are systematically later than the Sunspot number data as also seen in Table 4.

4.7 Period vs. amplitude

Significant relationships are also found between cycle periods and amplitudes. The most significant relationship is between a cycle period and the amplitude of the following cycle (Hathaway *et al.*, 1994; Solanki *et al.*, 2002). This is illustrated in Figure 27. The correlation is fairly strong ($r = -0.68$, $r^2 = 0.46$) and significant at the 99% level. While there is also a negative correlation between a cycle period and its own amplitude the correlation is much weaker ($r = -0.37$, $r^2 = 0.14$).

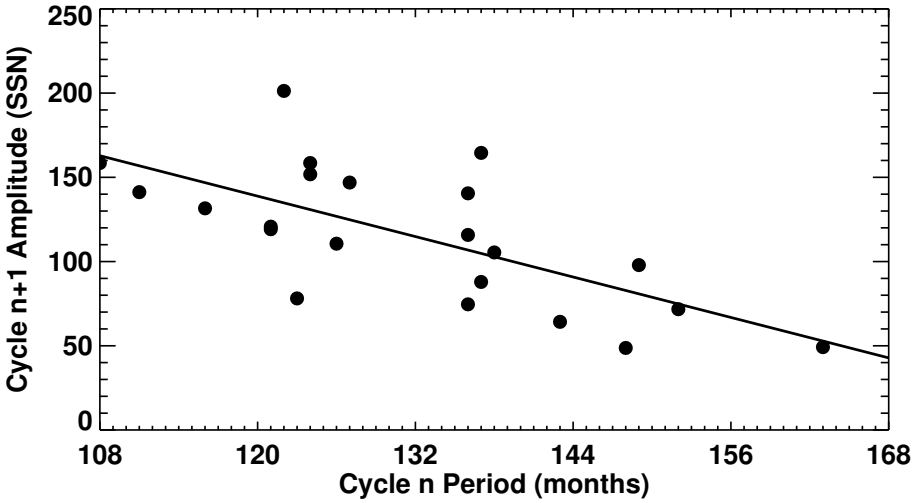

Figure 27: The Amplitude–Period Effect. The period of a cycle (from minimum to minimum) plotted versus following cycle amplitude for International Sunspot Number data from cycles 1 to 22. This gives an inverse relationship between amplitude and period shown by the solid with Amplitude(n+1) = 380 – 2 × Period(n).

4.8 Active latitudes

While Spörer's name is often attached to the concept of sunspot zones and their drift toward the equator, it appears that Carrington was the first to discover it. Carrington (1858) noted that the sunspots prior to the "minimum of frequency in February 1856" were confined to an equatorial band well below 20° latitude. He went on to note that after that date two new belts of sunspots appeared at latitudes between 20° and 40° latitude in each hemisphere. The RGO USAF/NOAA sunspot area and position data plotted in Figure 8 was used by Hathaway *et al.* (2003) to investigate the nature of this equatorward drift. The individual sunspot cycles can be separated near the time of minimum by the latitudes of the emerging sunspots (and more recently by magnetic polarity data as well). The centroid positions of the sunspot areas in each hemisphere are then calculated for each solar rotation. While Hathaway *et al.* (2003) investigated the latitude positions as functions of time relative to the date of maximum for each cycle, the data show far less scatter when plotted relative to the time of minimum. These centroid positions are plotted as functions of time relative to the date of minimum in Figure 28. The area weighted averages of these positions in 6-month intervals are shown with the colored lines for different amplitude cycles. Near minimum the centroid position of the sunspot areas is about 25° from the equator. The equatorward drift is more rapid early in the cycle and slows late in the cycle – eventually stopping at about 7° from the equator.

Cycle-to-cycle variations in this equatorward drift have been reported and latitudes of the sunspot zones have been related to cycle amplitudes. Vitinskij (1976) used the latitudes of sunspot

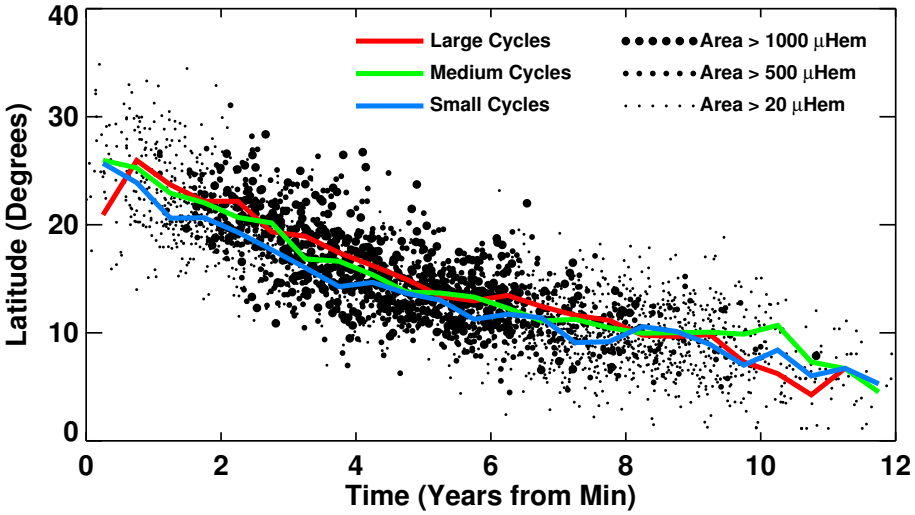

Figure 28: Latitude positions of the sunspot area centroid in each hemisphere for each Carrington Rotation as functions of time from cycle minimum. Three symbol sizes are used to differentiate data according to the daily average of the sunspot area for each hemisphere and rotation. The centroids of the centroids in 6-month intervals are shown with the red line for large amplitude cycles, with the green line for medium amplitude cycles, and with the blue line for the small amplitude cycles.

near minimum as a predictor for the amplitude of cycle 21. Separating the cycles according to size now suggests that this is a poor indicator of cycle amplitude. Regardless of amplitude class all cycles start with sunspot zones centered at about 25°. This is illustrated in Figure 28 where the latitude positions of the sunspot area centroids are shown for small amplitude cycles (cycles 12, 13, 14, and 16) in blue, for medium amplitude cycles (cycles 15, 17, 20, and 23) in green, and for large amplitude cycles (cycles 18, 19, 21, and 22) in red.

Becker (1954) and Waldmeier (1955) noted that in large cycles, the latitudes of the sunspot zones are higher at maximum than in small cycles. This is indicated in the data plotted in Figure 28. The sunspot zones in large amplitude cycles tend to stay at higher latitudes than in medium or small cycles from about a year after minimum to about five years after minimum. Since large amplitude cycles reach their maxima sooner than do medium or small amplitude cycles (the Waldmeier Effect – Section 4.6), the latitude differences are increased further.

The latitudinal width of the sunspot zones also varies over the cycle and as a function of cycle amplitude. This is illustrated in Figure 29 where the latitudinal widths of the sunspot zones are plotted for each hemisphere and Carrington rotation. The active latitude bands are narrow at minimum, expand to a maximum width at about the time of maximum, and then narrow again during the declining phase of the cycle. Larger cycles achieve greater widths than do smaller cycles. At all cycle phases and for all cycle amplitudes the active latitudes are fairly symmetrically centered with no systematic skew in the latitude distribution of sunspot areas.

4.9 Active hemispheres

Comparisons of the activity in each solar hemisphere show significant asymmetries. Spoerer (1889) and Maunder (1890, 1904) noted that there were often long periods of time when most of the sunspots were found preferentially in one hemisphere and not the other. Waldmeier (1971) found that this asymmetry extended to other measures of activity including faculae, prominences, and coronal brightness. Roy (1977) reported that major flares and magnetically complex sunspot

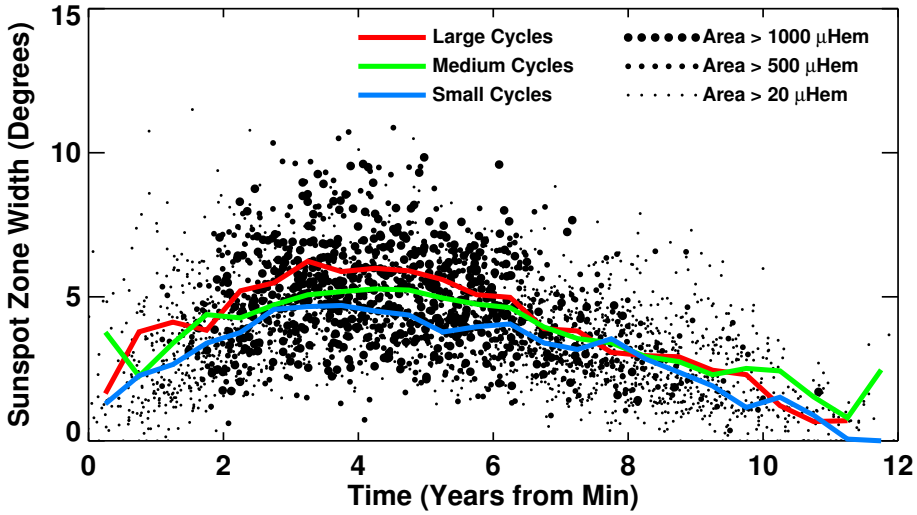

Figure 29: Latitudinal widths of the sunspot area centroid in each hemisphere for each Carrington Rotation as functions of time from cycle minimum. Three symbol sizes are used to differentiate data according to the daily average of the sunspot area for each hemisphere and rotation. The centroids of the centroids in 6-month intervals are shown with the red line for large amplitude cycles, with the green line for medium amplitude cycles, and with the blue line for the small amplitude cycles.

groups also showed strong north–south asymmetry. Simply quantifying the asymmetry itself is problematic. Taking the difference between hemispheric measures of activity (absolute asymmetry) produces strong signals around the times of maxima while taking the ratio of the difference to the sum (relative asymmetry) produces strong signals around the times of minima. Figure 30 shows the absolute asymmetry (North – South) of several key indicators. It is clear from this figure that hemispheric asymmetry is real (it consistently appears in all four indicators) and is often persistent – lasting for many years at a time. The absolute asymmetry in the RGO USAF/NOAA sunspot area smoothed with the 24-month Gaussian filter given by Equation (4) is shown in Figure 31. This indicates that north–south asymmetry can persist for years.

Systematic variations over the course of a solar cycle or as a function of cycle amplitude have been suggested but these variations have invariably been found to change from cycle to cycle (See Section 5). For example, Newton and Milsom (1955) showed that the northern hemisphere dominated in the early phases of cycles 12 – 15 with a switch to dominance in the south later in each cycle while the opposite was true for cycles 17 – 18. (This can be seen in Figure 31 where cycle 12 is the first cycle shown.) Waldmeier (1957, 1971) noted that a significant part of these variations can be accounted for by the fact that the two hemispheres are not exactly in phase. When the northern hemisphere activity leads that in the southern hemisphere, the north will dominate early in the cycle while the south will dominate in the declining phase. Carbonell *et al.* (1993) examined the relative asymmetry in sunspot areas with a variety of statistical tools and concluded that the signal is dominated by a random (and intermittent) component but contains a component that varies over a cycle and a component that gives long-term trends. The variation in the strength of the asymmetry over the course of an average cycle is strongly dependent upon how the asymmetry is quantified (strong at minimum for relative asymmetry, strong at maximum for absolute asymmetry). The variation from cycle-to-cycle will be discussed in Section 5.

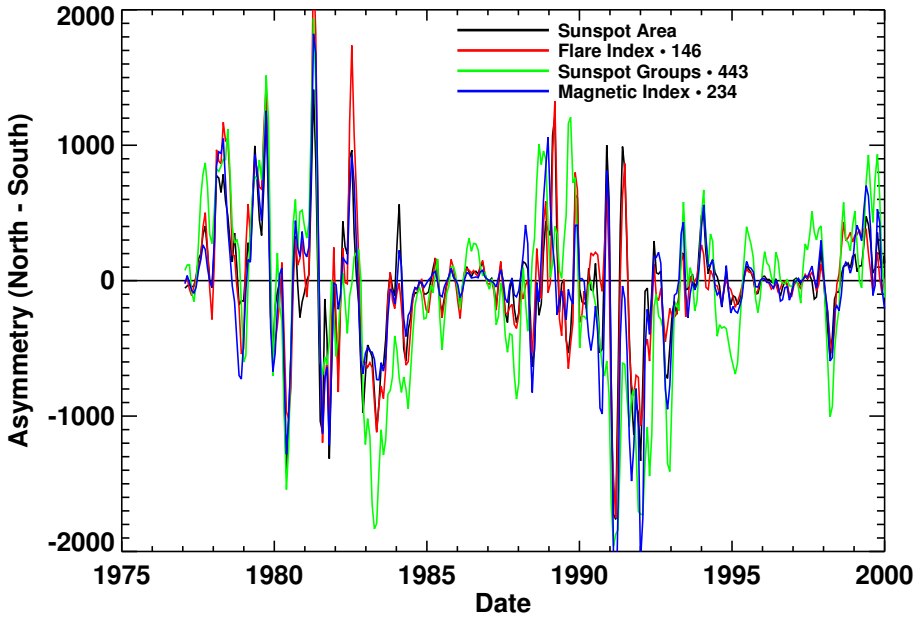

Figure 30: Absolute north–south asymmetry (North – South) in four different activity indicators. Sunspot area is plotted in black. The Flare Index scaled by 146 is shown in red. The number of sunspot groups scaled by 443 is shown in green. The Magnetic Index scaled by 234 is plotted in blue.

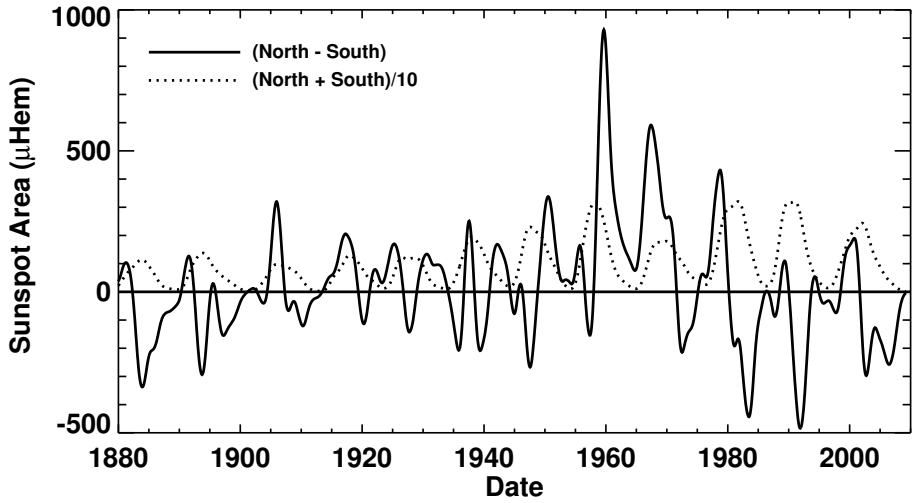

Figure 31: Smoothed north–south asymmetry in sunspot area. The hemispheric difference is shown with the solid line while the total area scaled by 1/10 is shown with the dotted line.

4.10 Active longitudes

Sunspots and solar activity also appear to cluster in "active longitudes." Early observers had noted that sunspot groups often emerge at the same positions as earlier groups. Bumba and Howard (1965) and Sawyer (1968) noted that new active regions grow in areas previously occupied by old active regions. Bogart (1982) found that this results in a periodic signal that is evident in the sunspot number record.

Figure 32 illustrates the active longitude phenomena. In Figure 32a the sunspot area in 5° longitude bins averaged over 1805 solar rotations since 1878 and normalized to the average value per bin is plotted as a function of Carrington longitude. The $2\,\sigma$ uncertainty in these values is represented by the dotted lines. This $2\,\sigma$ limit is reached at several longitudes and significantly exceeded at two ($85° - 90°$ and $90° - 95°$). Figure 32b shows similar data for each individual cycle with the normalized value offset in the vertical by the sunspot cycle number. There are many peaks at twice the normal value and one, in cycle 18 at $85° - 90°$, at three times the normal value. Some of these peaks even appear to persist from one cycle to the next, a result that has been noted by many authors including Bumba and Henja (1991), Miklailutsa and Makarova (1994), and Bai (2003). Henney and Harvey (2002) noted the persistence of magnetic structures in the northern hemisphere at preferred longitudes (drifting slightly due to the latitude) for two decades but also noted that (as seen in Figure 32b) that the sunspot records suggests that two decades is about the limit of such persistence.

Another interesting aspect of this phenomenon concerns the hemispheric differences. Berdyugina and Usoskin (2003) found that the active longitude in the northern hemisphere tends to be shifted by 180° in longitude from that in the southern hemisphere. This effect requires significant processing of the data to discern.

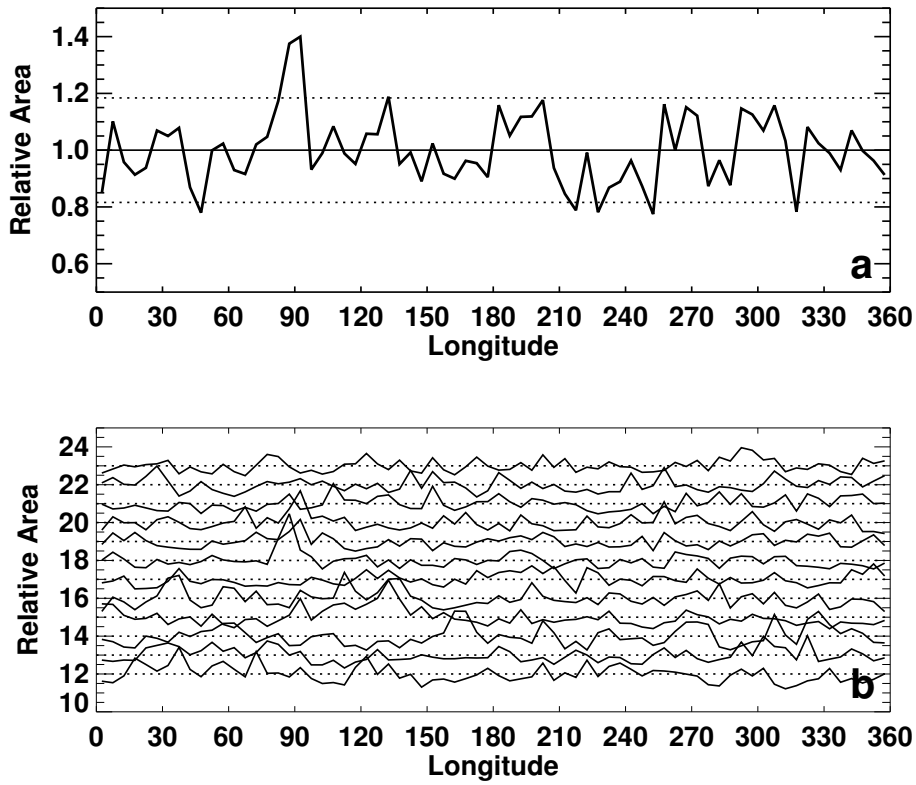

Figure 32: Active longitudes in sunspot area. The normalized sunspot area in 5° longitude bins is plotted in the upper panel (a) for the years 1878 – 2009. The dotted lines represent two standard errors in the normalized values. The sunspot area in several longitude bins meets or exceeds these limits. The individual cycles (12 through 23) are shown in the lower panel (b) with the normalized values offset in the vertical by the cycle number. Some active longitudes appear to persist from cycle to cycle.

5 Long-Term Variability

Systematic variations from cycle-to-cycle and over many cycles could be significant discriminators in models of the solar cycle and might aid in predicting future cycles. Several key aspects of long-term variability have been noted: a 70-year period of extremely low activity from 1645 to 1715 (the Maunder Minimum); a gradual increase in cycle amplitudes since the Maunder Minimum (a Secular Trend); an 80 – 90 year variation in cycle amplitudes (the Gleissberg Cycle); a two-cycle variation with odd numbered cycles higher than the preceding even numbered cycles (the Gnevyshev–Ohl Effect); a 205-year cycle in radio isotope proxies (the Suess Cycle); and other long term variations seen in radio isotopes. These aspects of long-term variability are examined in this section.

5.1 The Maunder Minimum

Maunder (1890) reporting on the work of Spörer noted that for a seventy year period from 1645 – 1715 the course of the sunspot cycle was interrupted. Eddy (1976) provided additional references to the lack of activity during this period and referred to it as the Maunder Minimum. He noted that many observers prior to 1890 had noticed this lack of activity and that both he and Maunder were simply pointing out an overlooked aspect of solar activity.

Hoyt and Schatten (1998) compiled observations from numerous sources to provide nearly complete coverage of sunspot observations during the period of the Maunder Minimum. These observations (Figure 33) clearly show the lack of activity and apparent cessation of the sunspot cycle during the Maunder Minimum. Nonetheless, Beer *et al.* (1998) find evidence for a weak cyclic variation in ^{10}Be during the Maunder Minimum suggesting that the magnetic cycle was still in progress but too weak to produce the intense magnetic fields in sunspots. In addition, Ribes and Nesme-Ribes (1993) found that the sunspot that were observed in the latter half of the Maunder Minimum were at low latitudes and dominant in the southern hemisphere – another indication of weak/marginal magnetic fields.

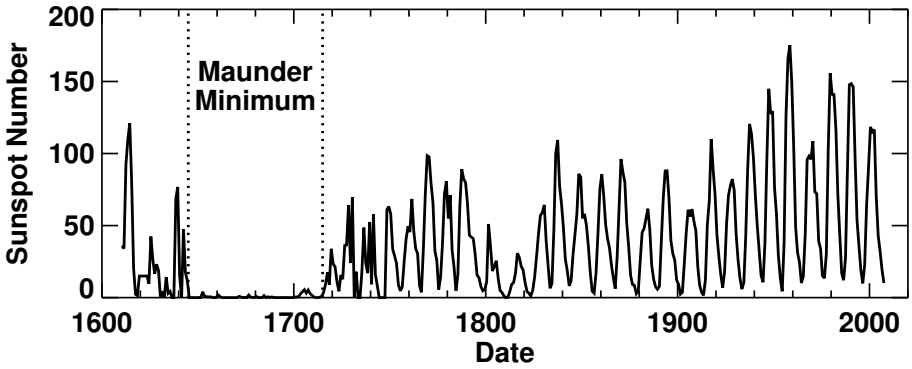

Figure 33: The Maunder Minimum. The yearly averages of the daily Group Sunspot Numbers are plotted as a function of time. The Maunder Minimum (1645 – 1715) is well observed in this dataset.

5.2 The secular trend

Since the Maunder Minimum there seems to have been a steady increase in sunspot cycle amplitudes (Wilson, 1988). This is readily seen in the yearly Group Sunspot Numbers plotted in Figure 33 and in the cycle amplitudes for Group Sunspot Numbers plotted in Figure 23. Hathaway *et al.* (2002) found a correlation coefficient of 0.7 between cycle amplitude and cycle number. This linear trend is not so apparent in the International Sunspot numbers plotted in Figure 23. It obviously cannot

continue forever but may represent an important characteristic of the solar cycle that should be represented in viable models for the cycle. Radioisotopes also show this recent trend (Solanki *et al.*, 2004) and indicate many upward and downward trends over the last 11,000 years.

5.3 The Gleissberg Cycle

Numerous authors have noted multi-cycle periodicities in the sunspot cycle amplitudes. Gleissberg (1939) noted a periodicity of seven or eight cycles in cycle amplitudes from 1750 to 1928. While Garcia and Mouradian (1998) suggest that a third period of this cycle can be found in the sunspot data, others (Hathaway *et al.*, 1999) suggest that the period is changing or (Rozelot, 1994; Ogurtsov *et al.*, 2002) that it consists of two different components (one with a 90 – 100 year period and a second with a 50 – 60 year period). A simple sinusoid fit to the residual cycle amplitudes when the secular trend is removed now gives a 9.1 cycle periodicity. This best fit is shown in Figure 34.

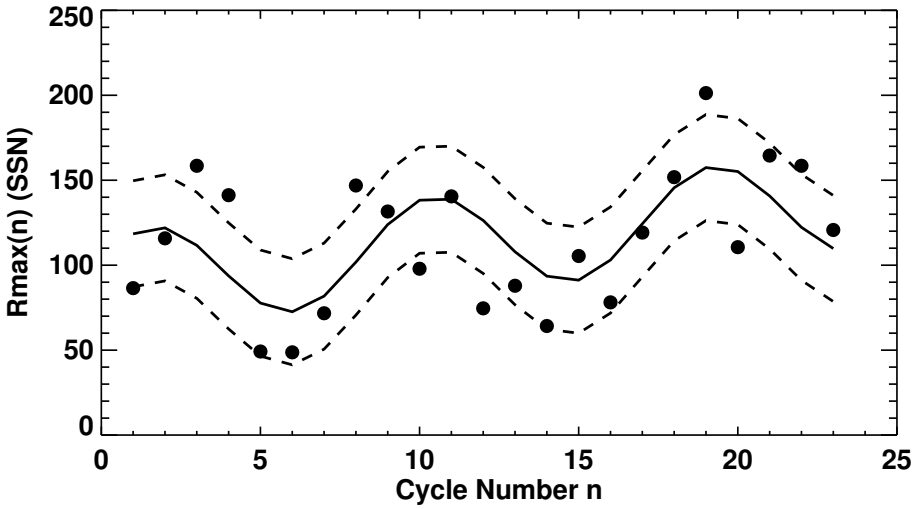

Figure 34: The Gleissberg Cycle. The best fit of cycle amplitudes to a simple sinusoidal function of cycle number is shown by the solid line (which includes the secular trend).

5.4 Gnevyshev–Ohl Rule (Even–Odd Effect)

Gnevyshev and Ohl (1948) found that if solar cycles are arranged in pairs with an even numbered cycle and the following odd numbered cycle then the sum of the sunspot numbers in the odd cycle is higher than in the even cycle. This is referred to as the Gnevyshev–Ohl Rule or Even–Odd Effect. This Rule is illustrated in Figure 35. With the exception of the Cycle 4/5 pair, this relationship held until cycle 23 showed that the cycle 22/23 pair was also an exception. If cycle amplitudes are compared then the Cycle 8/9 pair is also an exception. This rule also holds for other indicators of cycle amplitude such as sunspot area. While much has been said about this rule relative to the 22-year Hale cycle, it is difficult to understand why the order (even-odd vs. odd-even) of the pairing should make a difference. The observed effect does however impact flux transport models for the surface fields (see Sheeley Jr, 2005, for a review). Since the odd cycles all have the same magnetic polarity, stronger odd cycles will tend to build up polar fields of one polarity to the extent that the transport during the even cycles cannot reverse the polar fields without associated changes in transport.

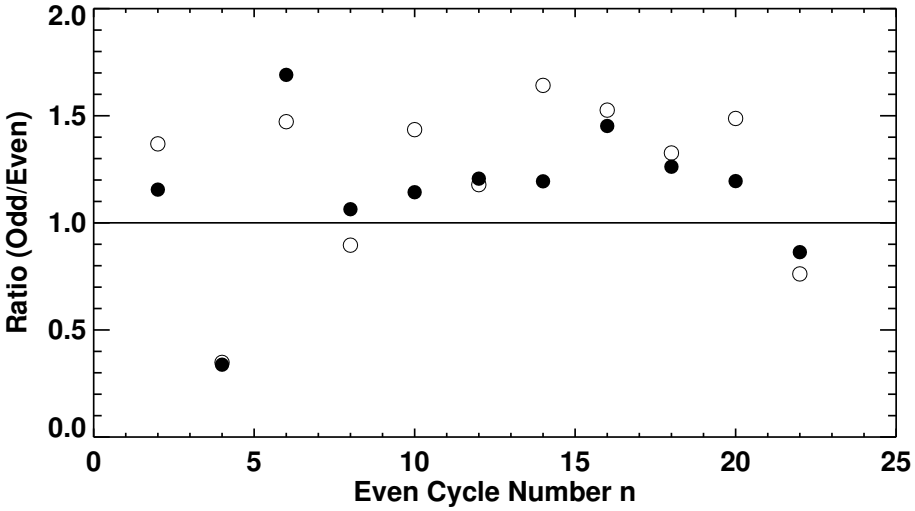

Figure 35: Gnevyshev–Ohl Rule. The ratio of the odd cycle sunspot sum to the preceding even cycle sunspot sum is shown with the filled circles. The ratio of the odd cycle amplitude to the preceding even cycle amplitude is shown with the open circles.

5.5 Long-term variations from radioisotope studies

The solar cycle modulation of cosmic rays (Section 3.8) leaves its imprint in the concentration of the radioisotopes ^{14}C in tree rings and ^{10}Be in ice cores (Section 3.9). The connection between solar activity and radioisotope concentrations is complicated by the transport and storage of these radioisotopes. Nonetheless, estimates of solar activity levels over time-scales much longer than the 400-year sunspot record can be obtained (see Usoskin, 2008, for a review).

These reconstructions of solar activity reveal Grand Minima like the Maunder Minimum as well as Grand Maxima similar to the last half of the 20th century. The reconstructions suggest that the Sun spends about 1/6th of its current life in a Grand Minimum phase and about 1/10th in a Grand Maximum.

5.6 The Suess cycle

One periodicity that arises in many radiocarbon studies of solar activity has a well defined period of about 210 years. This is often referred to as the Suess or de Vries Cycle (Suess, 1980). Although the variations in the calculated production rates of ^{14}C and ^{10}Be are well correlated with each other (Vonmoos *et al.*, 2006) and with the 400-year sunspot record (Berggren *et al.*, 2009), there is little evidence of the Suess Cycle in the sunspot record itself.

6 Short-Term Variability

There are significant variations in solar activity on time scales shorter than the sunspot cycle. This is evident when the sunspot number record is filtered to remove both solar rotation effects (periods of about 27-days and less) and solar cycle effects. This signal is shown in Figure 36 for the years 1850 – 2000. In this figure the daily sunspot numbers are filtered with a tapered Gaussian shaped filter (Equation (4)) with a FWHM of 54 days. This reduces all signals with periods shorter than 54-days to less than 2% of their original amplitude. The resulting signal is sampled at 27-day intervals and then filtered again with a similar Gaussian with a FWHM of 24 rotations. The lower panel of Figure 36 shows this final signal for the time period while the upper panel shows the residual obtained when this smoothed sunspot number signal is subtracted from 54-day filtered data. This residual signal is quite chaotic but shows some interesting behavior and quasi-periodicities.

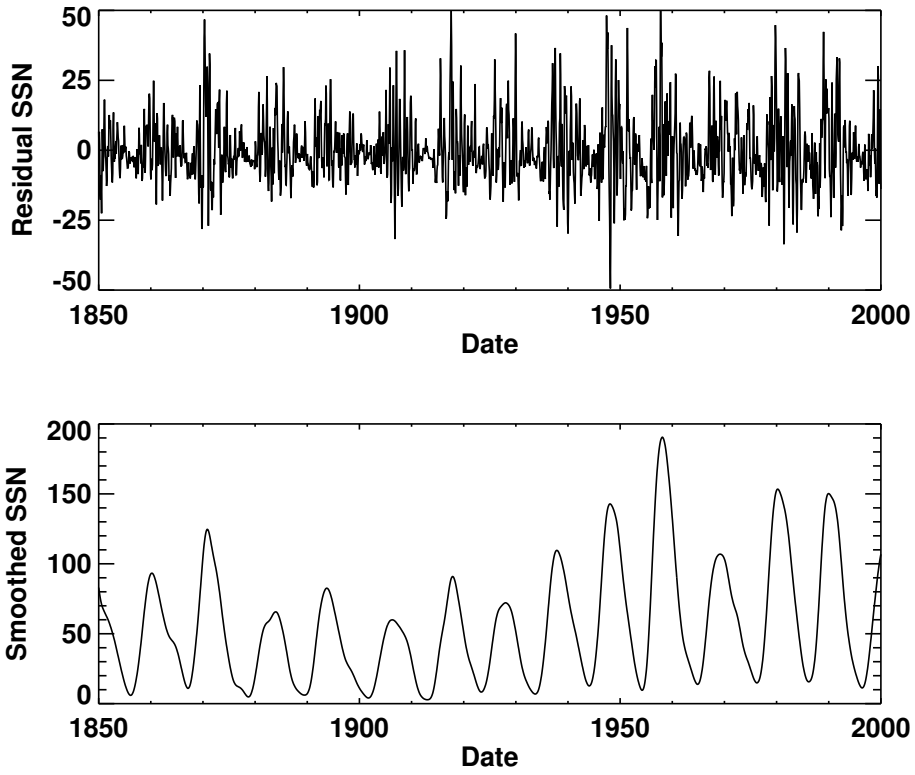

Figure 36: Short-term variations. The lower panel shows the daily International Sunspot Number (SSN) smoothed with a 24-rotation FWHM Gaussian. The upper panel shows the residual SSN signal smoothed with a 54-day Gaussian and sampled at 27-day intervals.

6.1 154-day periodicity

A 154 day periodic signal was noted in gamma-ray flare activity seen from SMM by Rieger *et al.* (1984) for the time interval from 1980/02 to 1983/08. This signal was also found by Bai and Cliver (1990) in proton flares for both this interval and an earlier interval from 1958/01 to 1971/12. Ballester *et al.* (2002) found that this signal was also seen in the Mt. Wilson sunspot index for the 1980 – 1983 time frame. Lean (1990) analyzed the signal in the sunspot area data and found

that it occurs in episodes around the epochs of sunspot cycle maxima and that its frequency drifts as well. A wavelet transform of the bandpass-limited (54 days $\lesssim$ period $\lesssim$ 2 years) daily sunspot numbers shown in the upper panel of Figure 36 is shown in Figure 37 with a horizontal red line indicating periods of 154 days. The strong signal in the early 1980s as well as other intermittent intervals is clearly evident in this plot.

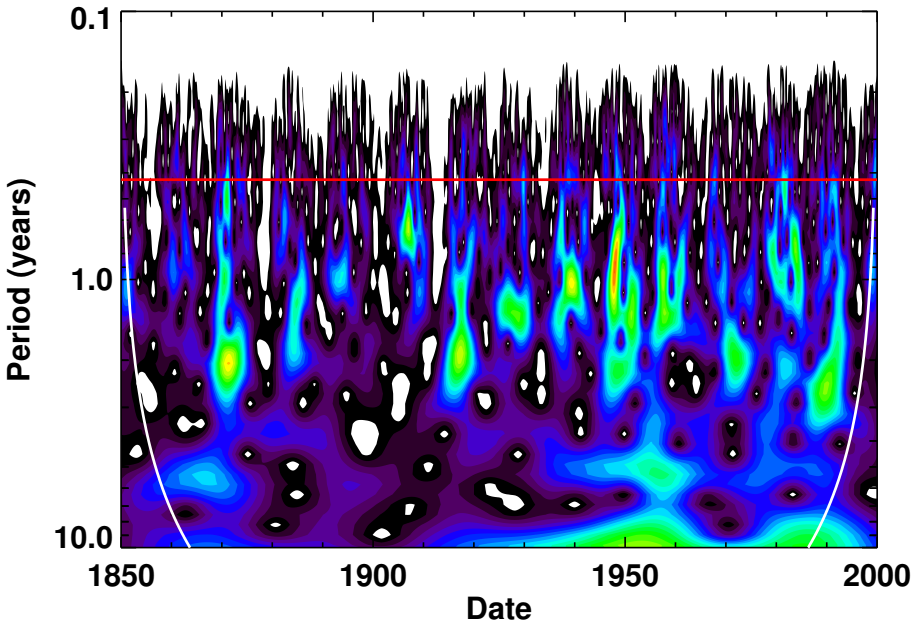

Figure 37: Morlet wavelet transform spectrum of the bandpass-limited daily International Sunspot Number. Increasing wavelet power is represented by colors from black through blue, green, and yellow to red. The Cone-Of-Influence is shown with the white curves. Periods of 154-days are indicated by the horizontal red line.

6.2 Quasi-biennial variations and double peaked maxima

Another interesting periodicity is one found with a period of about two years (Benevolenskaya, 1995; Mursula *et al.*, 2003). Many sunspot cycles exhibit double peaks when the monthly International Sunspot Number is smoothed with the traditional 13-month running mean. This was noted by Gnevyshev (1963, 1967, 1977) and often referred to as the Gnevyshev Gap. Wang and Sheeley Jr (2003) found that the Sun's dipole magnetic moment and open magnetic flux exhibits multiple peaks with quasi-periodicities of about 1.3 years that they attributed to the stochastic processes of active region emergence and a decay time of about 1 year set by the dynamical processes of differential rotation, meridional flow, and supergranule diffusion. These quasi-periodic variations are also evident in the wavelet spectrum shown in Figure 37. Multiple significant peaks of power are seen intermittently at periods between 1 and 2 years and are most prevalent near the time of cycle maxima (Bazilevskaya *et al.*, 2000). A signal with a similar period is seen in the Tachocline Oscillations – periodic variations in the shear at the base of the convection zone (Howe *et al.*, 2000). These tachocline oscillations have also been found to be intermittent (Howe *et al.*, 2007).

7 Solar Cycle Predictions

Predicting the solar cycle is indeed very difficult. A cursory examination of the sunspot record reveals a wide range of cycle amplitudes (Figure 2). Over the last 24 cycles the average amplitude (in terms of the 13-month-smoothed monthly averages of the daily sunspot number) was about 114. Over the last 400 years the cycle amplitudes have varied widely – from basically zero through the Maunder Minimum to the two small cycles of the Dalton Minimum at the start of the 19th century (amplitudes of 49.2 and 48.7) to the recent string of large cycles (amplitudes of 151.8, 201.3, 110.6, 164.5, 158.5, and 120.8). In addition to the changes in the amplitude of the cycle, there are changes in cycle length and cycle shape as discussed in Section 4.

7.1 Predicting an ongoing cycle

One popular and often used method for predicting solar activity was first described by McNish and Lincoln (1949). As a cycle progresses the smoothed monthly sunspot numbers are compared to the average cycle for the same number of months since minimum. The difference between the two is used to project future differences between predicted and mean cycle. The McNish–Lincoln regression technique originally used yearly values and only projected one year into the future. Later improvements to the technique use monthly values and use an auto-regression to predict the remainder of the cycle.

One problem with the modified McNish–Lincoln technique is that it does not account for systematic changes in the shape of the cycle with cycle amplitude (i.e. the Waldmeier Effect, Section 4.6). Another problem with the McNish–Lincoln method is its sensitivity to choices for the date of cycle minimum. Both the systematic changes in shape and the sensitivity to cycle minimum choice can be accounted for with techniques that fit the monthly data to parametric curves (e.g. Stewart and Panofsky, 1938; Elling and Schwentek, 1992; Hathaway *et al.*, 1994). The two-parameter function of Hathaway *et al.* (1994) (Equation (6)) closely mimics the changing shape of the sunspot cycle. Prediction requires fitting the data to the function with a best fit for an initial starting time, t_0, and amplitude, A.

Both the Modified McNish–Lincoln and the curve-fitting techniques work nicely once a sunspot cycle is well under way. The critical point seems to be 2 – 3 years after minimum near the time of the inflection point on the rise to maximum. Predictions for cycles 22 and 23 using the Modified McNish–Lincoln and the Hathaway, Wilson, and Reichmann curve-fitting techniques 24 months after minimum are shown in Figure 38. Since cycle 23 had an amplitude very close to the average of cycles 10 – 22, both of these predictions are very similar. Distinct differences are seen for larger or smaller cycles and when different dates are taken for minimum with the McNish–Lincoln method.

Predicting the size and timing of a cycle prior to its start (or even during the first year or two of the cycle) requires methods other than auto-regression or curve-fitting. There is a long, and growing, list of measured quantities that can and have been used to predict future cycle amplitudes. Prediction methods range from simple climatological means to physics-based dynamos with assimilated data.

7.2 Predicting future cycle amplitudes based on cycle statistics

The mean amplitude of the last n cycles gives the benchmark for other prediction techniques. The mean of the last 23 cycle amplitudes is 114.1 ± 40.4 where the error is the standard deviation about the mean. This represents a prediction without any skill. If other methods cannot predict with significantly better accuracy they have little use.

One class of prediction techniques is based on trends and periodicities in the cycle amplitudes. In general there has been an upward trend in cycle amplitudes since the Maunder Minimum.

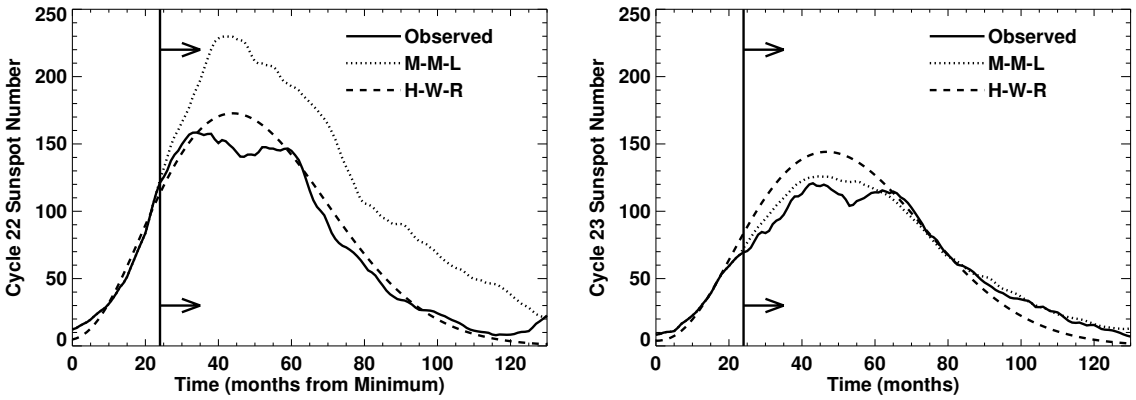

Figure 38: Predictions for cycles 22 and 23 using the Modified McNish–Lincoln (M-M-L) auto-regression technique and the Hathaway, Wilson, and Reichmann (H-W-R) curve-fitting technique 24 months after the minima for each cycle.

Projecting this trend to the next cycle gives a prediction slightly better than the mean. A number of periodicities have been noted in the cycle amplitude record. Gleissberg (1939) noted a long-period variation in cycle amplitudes with a period of seven or eight cycles (Section 5.3 and Figure 34). Gnevyshev and Ohl (1948) noted a two-cycle periodicity with the odd numbered cycle having larger amplitude than the preceding even numbered cycle (Section 5.4 and Figure 35). Ahluwalia (1998) noted a three-cycle sawtooth shaped periodicity in the six-cycle record of the geomagnetic Ap index.

Another class of prediction techniques uses the characteristics of the preceding cycle as indicators of the size of the next cycle. Wilson *et al.* (1998) found that the length (period) of the preceding cycle is inversely correlated to the amplitude of the following cycle. Another indicator of the size of the next cycle is the level of activity at minimum – the amplitude of the following cycle is correlated with the smoothed sunspot number at the preceding minimum (Brown, 1976). This type of technique has led to searches for activity indicators that are correlated with future cycle amplitude. Javaraiah (2007), for example, has found sunspot areas from intervals of time and latitude that correlate very well with future cycle activity.

7.3 Predicting future cycle amplitudes based on geomagnetic precursors

One class of precursors for future cycle amplitudes that has worked well in the past uses geomagnetic activity during the preceding cycle or near the time of minimum as an indicator of the amplitude for the next cycle. These "Geomagnetic Precursors" use indices for geomagnetic activity (see Section 3.7) that extend back to 1844. Ohl (1966) found that the minimum level of geomagnetic activity seen in the aa index near the time of sunspot cycle minimum was a good predictor for the amplitude of the next cycle. This is illustrated in Figure 39. The minima in aa are well defined and are well correlated with the following sunspot number maxima ($r = 0.93$). The ratio of $\max(R)$ to $\min(aa)$ gives

$$\max(R) = 7.95\,\min(aa) \pm 18 \tag{8}$$

This standard deviation from the relationship is significantly smaller than that associated with the average cycle prediction. The current (declining) level of the smoothed aa index indicates a small cycle 24 – $R_{\max}(24) = 78 \pm 18$. One problem with this method concerns the timing of the aa index minima – they often occur well after sunspot cycle minimum and therefore do not give a much advanced prediction.

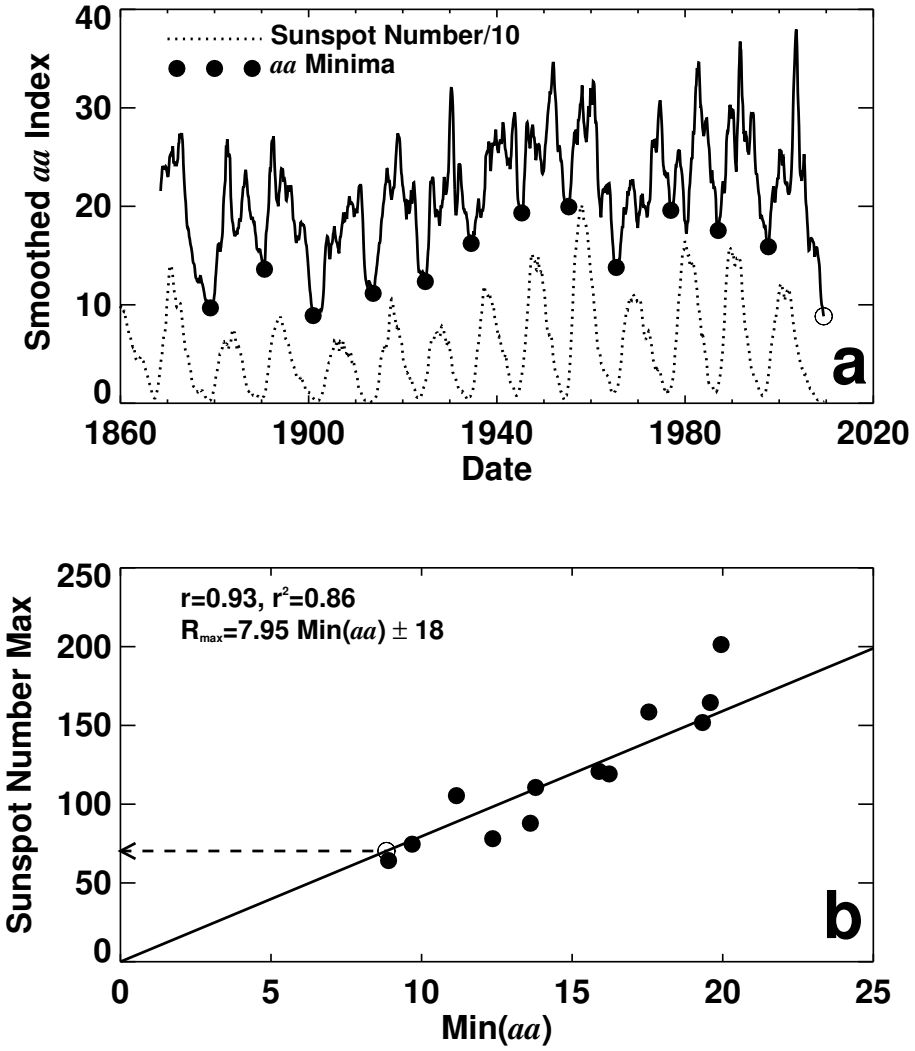

Figure 39: Ohl's method for predicting cycle amplitudes using the minima in the smoothed *aa* index (panel a) as precursors for the maximum sunspot numbers of the following sunspot number maxima (panel b).

Two variations on this method circumvent the timing problem. Feynman (1982) noted that geomagnetic activity has two different sources – one due to solar activity (flares, CMEs, and filament eruptions) that follows the sunspot cycle and another due to recurrent high speed solar wind streams that peaks during the decline of each cycle (see Section 3.7 and Figures 18 and 19). She separated the two by finding the sunspot number dependence of the base level of geomagnetic activity and removing it to reveal the "interplanetary" component of geomagnetic activity. The peaks in the interplanetary component prior to sunspot cycle minimum are very good indicators for the amplitude of the following sunspot cycle as shown in Figure 40.

Hathaway and Wilson (2006) used a modification of this method to predict cycle 24. At the time of that writing there was a distinct peak in $aa_{\rm I}$ in late 2003. This large peak led to a prediction of $R_{\rm max}(24) = 160 \pm 25$. While this method does give predictions prior to sunspot number minimum it is not without its problems. Different smoothings of the data give very different maxima and different methods are used to extract the sunspot number component for the data shown in Figure 39a. Feynman (1982) and others chose to pass a sloping line through the two lowest points. Hathaway and Wilson (2006) fit a line through the 20 lowest points from 20 bins in sunspot number. These variations introduce significant uncertainty in the actual predictions.

Thompson (1993) also noted that some geomagnetic activity during the previous cycle served as a predictor for the amplitude of the following cycle but, instead of trying to separate the two, he simply related the geomagnetic activity (as represented by the number of days with the geomagnetic Ap index ≥ 25) during one cycle to the sum of the amplitudes of that cycle and the following cycle (Figure 41). Predictions for the amplitude of a sunspot cycle are available well before minimum with this method. The number of geomagnetically disturbed days during cycle 23 gives a prediction of $R_{\rm max}(24) = 131 \pm 28$. Disadvantages with this method include the fact that two cycle amplitudes are involved, the fact that longer cycle will have more disturbed days simply due to their length, and the standard errors are larger.

Hathaway *et al.* (1999) tested these precursor methods by backing-up in time to 1950, calibrating each precursor method using only data prior to the time, and then using each method to predict cycles 19 – 22, updating the data and recalibrating each method for each remaining cycle. The results of this test were examined for both accuracy and stability (i.e. did the relationships used in the method vary significantly from one cycle to the next). An updated (including cycle 23 and corrections to the data) version of their Table 3 is given here as Table 6. The RMS errors in the predictions show that the geomagnetic precursor methods (Ohl's method, Feynman's method, and Thompson's method) consistently outperform the other tested methods. Furthermore, these geomagnetic precursor methods are also more stable. For example, as time progressed from cycle 19 to cycle 23 the Gleissberg cycle period changed from 7.5-cycles to 8.5-cycles and the mean cycle amplitude changed from 103.9 to 114.1 while the relationships between geomagnetic indicators and sunspot cycle amplitude were relatively unchanged.

The physics behind the geomagnetic precursors is uncertain. The geomagnetic disturbances that produce the precursor signal are primarily due to high speed solar wind streams from low latitude coronal holes late in a cycle. Schatten and Sofia (1987) suggested that this geomagnetic activity near the time of sunspot cycle minimum is related to the strength of the Sun's polar magnetic field which is, in turn, related to the strength of the following maximum (see next Section 7.4 on dynamo based predictions). Cameron and Schüssler (2007) suggest that it is simply the overlap of the sunspot cycles and the Waldmeier Effect that leads to these precursor relationships with the next cycle's amplitude. Wang and Sheeley Jr (2009) argue that Ohl's method has closer connections to the Sun's magnetic dipole strength and should therefore provide better predictions.

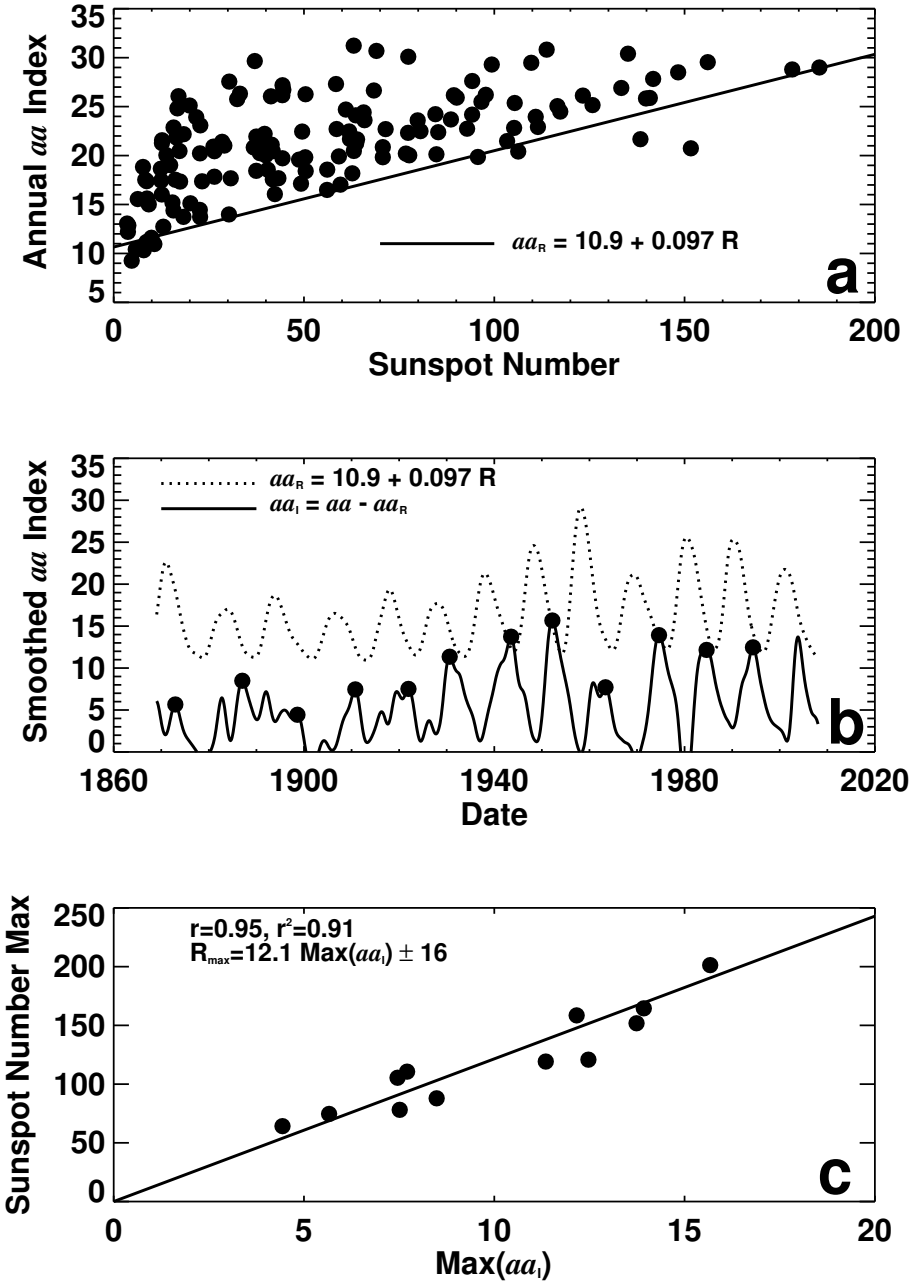

Figure 40: A modification of Feynman's method for separating geomagnetic activity into a sunspot number related component and an "Interplanetary" component (panels a and b). The maxima in aa_I prior to minimum are well correlated with the following sunspot number maxima (panel c).

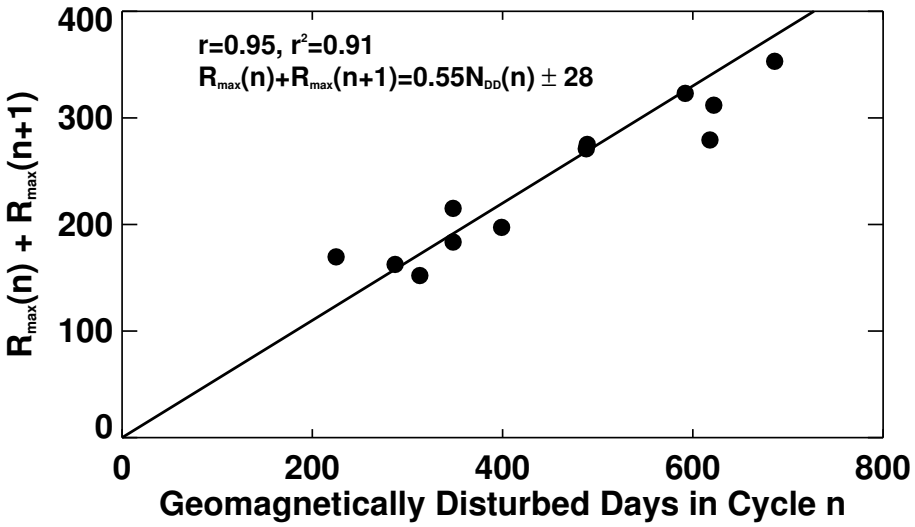

Figure 41: Thompson method for predicting sunspot number maxima. The number of geomagnetically disturbed days in a cycle is proportional to the sum of the maxima of that cycle and the next.

Table 6: Prediction method errors for cycle 19 – 23. The three geomagnetic precursor methods (Ohl's, Feynman's, and Thompson's) give the smallest errors.

Prediction Method	cycle 19	cycle 20	cycle 21	cycle 22	cycle 23	RMS
Mean Cycle	–97.4	–1.6	–55.4	–46.7	–6.9	54.4
Even–Odd	–60.1	?	–26.7	?	61.4	52.0
Maximum–Minimum	–109.7	24.9	–18.6	–8.1	5.2	51.2
Amplitude–Period	–75.3	18.4	–73.5	–25.6	15.0	49.6
Secular Trend	–96.4	14.6	–40.6	–25.4	18.9	49.3
Three Cycle Sawtooth	–96.5	14.6	–38.5	–25.4	18.8	49.0
Gleissberg Cycle	–64.8	48.0	–36.9	–31.8	–0.9	42.1
Ohl's Method	–55.4	–5.9	2.3	–9.1	10.5	28.7
Feynman's Method	–43.3	–22.4	–1.0	–14.8	25.9	28.6
Thompson's Method	–17.8	8.7	–26.5	–13.6	40.5	27.0

7.4 Predicting future cycle amplitudes based on dynamo theory

Dynamo models for the Sun's magnetic field and its evolution have led to predictions based on aspects of those models. Schatten *et al.* (1978) suggested using the strength of the Sun's polar field as a predictor for the amplitude of the following cycle based on the Babcock (1961) dynamo model. In the Babcock model the polar field at minimum is representative of the poloidal field that is sheared out by differential rotation to produce the toroidal field that erupts as active regions during the following cycle. Diffusion of the erupting active region magnetic field and transport by the meridional flow (along with the Joy's Law tilt of these active regions) then leads to the accumulation of opposite polarity fields at the poles and the ultimate reversal of the polar fields as shown in Figure 15.

Good measurements of the Sun's polar field are difficult to obtain. The field is weak and predominantly radially directed and thus nearly transverse to our line-of-sight. This makes the Zeeman signature weak and prone to the detrimental effects of scattered light. Nevertheless, systematic measurements of the polar fields have been made at the Wilcox Solar Observatory since 1976 and have been used by Schatten and his colleagues to predict cycles 21 – 24. These polar field measurements are shown in Figure 42 along with smoothed sunspot numbers. While the physical basis for these predictions is appealing, the fact that the necessary measurements are only available for the last three cycles is a distinct problem. It is unclear when the measurements should be taken. Predictions by this group for previous cycles have given different values at different times. The RMS differences between the published predictions and the observed cycle amplitudes suggest that these predictions are about as good as the geomagnetic precursor predictions. The polar fields are obviously much weaker during the current minimum. This has led to a prediction of $R_{\max}(24) = 75 \pm 8$ by Svalgaard *et al.* (2005) – about half the size of the previous three cycles based on the polar fields being about half as strong. While in previous minima the strength of the polar fields (as represented by the average of the absolute field strength in the north and in the south) varied as minimum approached, this did not happen on the approach to cycle 24 minimum in late 2008. This suggests that the prediction made in 2005 still holds.

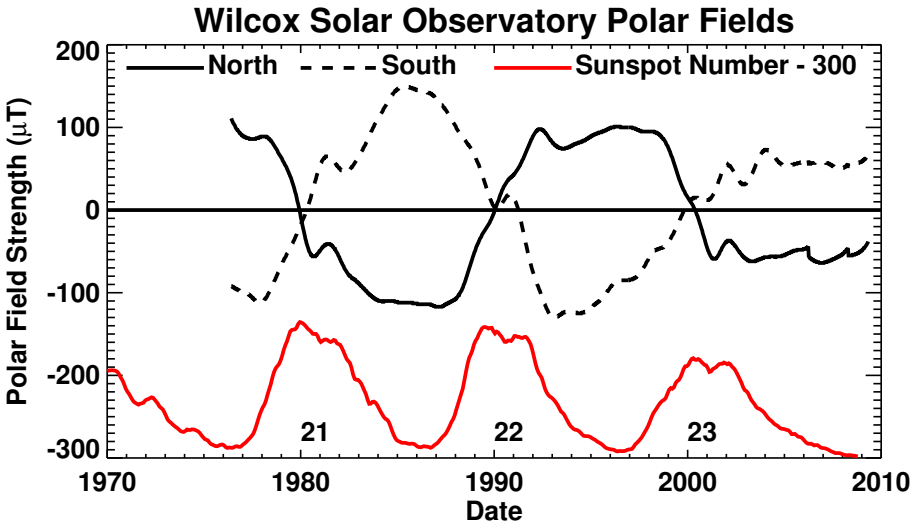

Figure 42: Polar magnetic fields as measured at the Wilcox Solar Observatory. The average of the north and south field strengths near the time of sunspot cycle minimum is expected to be an indicator for the amplitude of the next sunspot cycle.

Over the last decade dynamo models have started to include the effect of the Sun's meridional

circulation and found that it can play a significant role in the magnetic dynamo (cf. Dikpati and Charbonneau, 1999). In these models the speed of the meridional circulation sets the cycle period and influences both the strength of the polar fields and the amplitudes of following cycles. Two predictions have recently been made based on flux transport dynamos with assimilated data – with very different results.

Dikpati *et al.* (2006) predicted an amplitude for cycle 24 of 150 – 180 using a flux transport dynamo that included a rotation profile and a near surface meridional flow based on helioseismic observations. They modeled the axisymmetric poloidal and toroidal magnetic field using a meridional flow that returns to the equator at the base of the convection zone and used two source terms for the poloidal field – one at the surface due to the Joy's Law tilt of the emerging active regions and one in the tachocline due to hydrodynamic and MHD instabilities. The diffusivity in the model is a function of depth with a surface diffusivity of 5×10^{12} cm^2 s^{-1} falling to 5×10^{10} cm^2 s^{-1} at $r = 0.9\,R_\odot$. They drive the model with a surface source of poloidal field that depends upon the sunspot areas observed since 1874. Measurements of the meridional flow speed prior to 1996 are highly uncertain (cf. Hathaway, 1996) so they maintained a constant flow speed prior to 1996 and forced each of those earlier cycles to have a constant period as a consequence. The surface poloidal source term drifted linearly from 30° to 5° over each cycle with an amplitude that depended on the observed sunspot areas. They based their prediction on the strength of the toroidal field produced in the tachocline. They found excellent agreement between this toroidal field strength and the amplitude of each of the last eight cycles (the four earlier cycles – during the initialization phase – were also well fit but not with the degree of agreement of the later cycles). The correlation they find between the predicted toroidal field and the cycle amplitudes is similar to that found with the geomagnetic precursors and polar field strength indicators. When they kept the meridional flow speed at the same constant level during cycle 23 they found $R_{\max}(24) \sim 180$. When they allowed the meridional flow speed to drop by 40% as was seen from 1996 – 2002 they found $R_{\max}(24) \sim 150$ and further predicted that cycle 24 would start late.

Choudhuri *et al.* (2007) predicted an amplitude for cycle 24 of 80 using a similar flux-transport dynamo but with the surface poloidal field at minimum as the assimilated data. They used a similar axisymmetric model for the poloidal and toroidal fields but with a meridional flow that extends below the base of the convection zone and a diffusivity that remains high throughout the convection zone. In their model the toroidal field in the tachocline produces flux eruptions when its strength exceeds a given limit. They compare the number of eruptions to the observed sunspot numbers and use this as the predictor for cycle 24. They assimilate data by instantaneously changing the poloidal field at minimum throughout most of the convection zone to make it match the dipole moment obtained from the Wilcox Solar Observatory observations (Figure 41). They found an excellent fit to the last three cycles (the full extent of the data) and found $R_{\max}(24) \sim 80$, in agreement with the polar field prediction of Svalgaard *et al.* (2005).

Criticism has been leveled against all of these dynamo-based predictions. Dikpati *et al.* (2006) criticized the use of polar field strengths to predict the sunspot cycle peak that follows by four years by questioning how those fields could be carried down to the low latitude tachocline in such a short time. Cameron and Schüssler (2007) produced a simplified 1D flux transport model and showed that with similar parameters to those used by Dikpati *et al.* (2006) the flux transport across the equator was an excellent predictor for the amplitude of the next cycle but the predictive skill was lost when more realistic parameterizations of the active region emergence were used. Yeates *et al.* (2008) compared an advection-dominated model like that of Dikpati *et al.* (2006) to a diffusion-dominated models like that of Choudhuri *et al.* (2007) and concluded that the diffusion-dominated model was better because it gave a better fit to the relationship between meridional flow speed and cycle amplitude. Dikpati *et al.* (2008a) returned with a study of the use of polar fields and cross equatorial flux as predictors of cycle amplitudes and concluded that their tachocline toroidal flux was the best indicator. Furthermore, they found that the polar fields followed the current

cycle so that the weak polar fields at this minimum are due to the weakened meridional flow. The strongest criticism of these dynamo-based predictions was give by Tobias *et al.* (2006) and Bushby and Tobias (2007). They conclude that the solar dynamo is deterministically chaotic and thus inherently unpredictable.

8 Conclusions

Understanding the solar cycle remains as one of the biggest problems in solar physics. It is also one of the oldest. Several key features of the solar cycle have been reviewed here and must be explained by any viable theory or model.

- The solar cycle has a period of about 11 years but varies in length with a standard deviation of about 14 months.
- Each cycle appears as an outburst of activity that overlaps with both the preceding and following cycles by about 18 months.
- Solar cycles are asymmetric with respect to their maxima – the rise to maximum is shorter than the decline to minimum and the rise time is shorter for larger amplitude cycles.
- Big cycles usually start early and leave behind a short preceding cycle and a high minimum of activity.
- Sunspots erupt in low latitude bands on either side of the equator and these bands drift toward the equator as each cycle progresses.
- The activity bands widen during the rise to maximum and narrow during the decline to minimum.
- At any time one hemisphere may dominate over the other but the northern and southern hemispheres never get completely out of phase.
- Sunspots erupt in groups extended in longitude but more constrained in latitude with one magnetic polarity associated with the leading (in the direction of rotation) spots and the opposite polarity associated with the following spots.
- The magnetic polarities of active regions reverse from northern to southern hemispheres and from one cycle to the next.
- The polar fields reverse polarity during each cycle at about the time of cycle maximum.
- The leading spots in a group are positioned slightly equatorward of the following spots and this tilt increases with latitude.
- Cycle amplitudes exhibit weak quasi-periodicities like the 7 to 8-cycle Gleissberg Cycle.
- Cycle amplitudes exhibit extended periods of inactivity like the Maunder Minimum.
- Solar activity exhibits quasi-periodicities at time scales shorter than 11 years.
- Predicting the level of solar activity for the remainder of a cycle is reliable 2 – 3 years after cycle minimum.
- Predictions for the amplitude of a cycle based on the Sun's polar field strength or on geomagnetic activity near cycle minimum are significantly better than using the climatological mean.

References

Abbot, C.G., Fowle, F.E. and Aldrich, L.B., 1913, "The Variation of the Sun", *Astrophys. J.*, **38**, 181–186. [DOI], [ADS] (Cited on page 14.)

Ahluwalia, H.S., 1998, "The predicted size of cycle 23 based on the inferred three-cycle quasi-periodicity of the planetary index *Ap*", *J. Geophys. Res.*, **103**(A6), 12,103–12,109. [DOI], [ADS] (Cited on page 48.)

Babcock, H.D., 1959, "The Sun's Polar Magnetic Field", *Astrophys. J.*, **130**, 364–365. [DOI], [ADS] (Cited on page 17.)

Babcock, H.W., 1961, "The topology of the Sun's magnetic field and the 22-year cycle", *Astrophys. J.*, **133**, 572–587. [DOI], [ADS] (Cited on page 53.)

Bachmann, K.T. and White, O.R., 1994, "Observations of Hysteresis in Solar Cycle Variations Among Seven Solar Activity Indicators", *Solar Phys.*, **150**, 347–357. [DOI], [ADS] (Cited on pages 14 and 34.)

Bai, T., 2003, "Hot Spots for Solar Flares Persisting for Decades: Longitude Distributions of Flares of Cycles 19-23", *Astrophys. J.*, **585**, 1114–1123. [DOI], [ADS] (Cited on page 40.)

Bai, T. and Cliver, E.W., 1990, "A 154 Day Periodicity in the Occurrence Rate of Proton Flares", *Astrophys. J.*, **363**, 299–309. [DOI], [ADS] (Cited on page 45.)

Ballester, J.L., Oliver, R. and Carbonell, M., 2002, "The Near 160 Day Periodicity in the Photospheric Magnetic Flux", *Astrophys. J.*, **566**, 505–511. [DOI], [ADS] (Cited on page 45.)

Balmaceda, L.A., Solanki, S.K., Krivova, N.A. and Foster, S., 2009, "A homogeneous database of sunspot areas covering more than 130 years", *J. Geophys. Res.*, **114**, A07104. [DOI], [ADS], [arXiv:0906.0942] (Cited on page 11.)

Baranyi, T., Gyõri, L., Ludmány, A. and Coffey, H.E., 2001, "Comparison of sunspot area data bases", *Mon. Not. R. Astron. Soc.*, **323**, 223–230. [DOI], [ADS] (Cited on page 11.)

Bazilevskaya, G.A., Krainev, M.B., Makhmutov, V.S., Flückiger, E.O. and Sladkova, A.I. Storini, M., 2000, "Structure and Maximum Phase of Solar Cycles 21 and 22", *Solar Phys.*, **197**, 157–174. [DOI], [ADS] (Cited on page 46.)

Becker, U., 1954, "Die Eigenbewegung der Sonnenflecken in Breite", *Z. Astrophys.*, **34**, 129–136. [ADS] (Cited on page 37.)

Beer, J., Blinov, A., Bonani, G., Finkel, R.C., Hofmann, H.J., Lehmann, B., Oeschger, H., Sigg, A., Schwander, J., Staffelbach, T., Stauffer, B., Suter, M. and Wötfli, W., 1990, "Use of ^{10}Be in polar ice to trace the 11-year cycle of solar activity", *Nature*, **347**, 164–166. [DOI], [ADS] (Cited on page 24.)

Beer, J., Tobias, S. and Weiss, N., 1998, "An active Sun throughout the Maunder Minimum", *Solar Phys.*, **181**, 237–249. [DOI], [ADS] (Cited on page 42.)

Benevolenskaya, E.E., 1995, "Double Magnetic Cycle of Solar Activity", *Solar Phys.*, **161**, 1–8. [DOI], [ADS] (Cited on page 46.)

Benz, A.O., 2008, "Flare Observations", *Living Rev. Solar Phys.*, **5**, lrsp-2008-1. URL (cited on 3 February 2010):
http://www.livingreviews.org/lrsp-2008-1 (Cited on page 18.)

Berdyugina, S.V. and Usoskin, I.G., 2003, "Active longitudes in sunspot activity: Century scale Persistence", *Astron. Astrophys.*, **405**, 1121–1128. [DOI], [ADS] (Cited on page 40.)

Berggren, A.-M., Beer, J., Possnertt, G., Aldahan, A., Kubik, P., Christl, M., Johnsen, S.J., Abreu, J. and Vinther, B.M., 2009, "A 600-year annual ^{10}Be record from the NGRIP ice core, Greenland", *Geophys. Res. Lett.*, **36**, L11801. [DOI], [ADS] (Cited on page 44.)

Bogart, R.S., 1982, "Recurrence of Solar Activity: Evidence for Active Longitudes", *Solar Phys.*, **76**, 155–165. [DOI], [ADS] (Cited on page 40.)

Bray, R.J. and Loughhead, R.E., 1965, *Sunspots*, Wiley, New York (Cited on page 6.)

Brown, G.M., 1976, "What determines sunspot maximum?", *Mon. Not. R. Astron. Soc.*, **174**, 185–189. [ADS] (Cited on page 48.)

Bumba, V. and Henja, L., 1991, "Low-latitude Active Longitudes on the Sun and in Interplanetary Space", *Bull. Astron. Inst. Czech.*, **42**, 76–84. [ADS] (Cited on page 40.)

Bumba, V. and Howard, R., 1965, "Large-scale Distribution of Solar Magnetic Fields", *Astrophys. J.*, **141**, 1502–1512. [DOI], [ADS] (Cited on page 40.)

Bushby, P.J. and Tobias, S.T., 2007, "On predicting the solar cycle using mean-field models", *Astrophys. J.*, **661**, 1289–1296. [DOI], [ADS] (Cited on page 55.)

Cameron, R. and Schüssler, M., 2007, "Solar cycle prediction using precursors and flux transport models", *Astrophys. J.*, **659**, 801–811. [DOI], [ADS] (Cited on pages 50 and 54.)

Carbonell, M., Oliver, R. and Ballester, J.L., 1993, "On the asymmetry of solar activity", *Astron. Astrophys.*, **274**, 497–504. [ADS] (Cited on page 38.)

Carrington, R.C., 1858, "On the Distribution of the Solar Spots in Latitude Since the Beginning of the Year 1854; with a map", *Mon. Not. R. Astron. Soc.*, **19**, 1–3. [ADS] (Cited on page 36.)

Carrington, R.C., 1859, "Description of a Singular Appearance seen in the Sun on September 1, 1859", *Mon. Not. R. Astron. Soc.*, **20**, 13–15. [ADS] (Cited on page 18.)

Charbonneau, P., 2005, "Dynamo Models of the Solar Cycle", *Living Rev. Solar Phys.*, **2**, lrsp-2005-2. URL (cited on 3 February 2010):
http://www.livingreviews.org/lrsp-2005-2 (Cited on page 5.)

Choudhuri, A.R., Chatterjee, P. and Jiang, J., 2007, "Predicting solar cycle 24 with a solar dynamo model", *Phys. Rev. Lett.*, **98**, 131103. [DOI], [ADS] (Cited on page 54.)

Clark, D.H. and Stephenson, F.R., 1978, "An Interpretation of Pre-Telescopic Records from the Orient", *Quart. J. R. Astron. Soc.*, **19**, 387–410. [ADS] (Cited on page 6.)

Dikpati, M. and Charbonneau, P., 1999, "A Babcock-Leighton flux transport dynamo with solar-like differential rotation", *Astrophys. J.*, **518**, 508–520. [DOI], [ADS] (Cited on page 54.)

Dikpati, M., de Toma, G. and Gilman, P.A., 2006, "Predicting the strength of solar cycle 24 using a flux-transport dynamo-based tool", *Geophys. Res. Lett.*, **33**, L05102. [DOI], [ADS] (Cited on page 54.)

Dikpati, M., de Toma, G. and Gilman, P.A., 2008a, "Polar flux, cross-equatorial flux, and dynamo generated tachocline toroidal flux as predictors of solar cycles", *Astrophys. J.*, **675**, 920–930. [DOI], [ADS] (Cited on page 54.)

Dikpati, M., Gilman, P.A. and de Toma, G., 2008b, "The Waldmeier Effect: An Artifact of the Definition of Wolf Sunspot Number?", *Astrophys. J. Lett.*, **673**, L99–L101. [DOI], [ADS] (Cited on page 34.)

"Latest Solar Radio Flux Report", project homepage, Space Weather Canada. URL (cited on 3 February 2010):
hhttp://www.spaceweather.ca/sx-4-eng.php (Cited on page 14.)

Eddy, J.A., 1976, "The Maunder Minimum", *Science*, **192**, 1189–1202. [DOI], [ADS] (Cited on page 42.)

Eddy, J.A., 1977, "Historical evidence for the existence of the solar cycle", in *The Solar Output and Its Variation*, (Ed.) White, O.R., Proceedings of a Workshop, held in Boulder, Colorado, April 26 – 28, 1976, pp. 55–71, Colorado Associated University Press, Boulder, CO. [ADS] (Cited on page 31.)

Elling, W. and Schwentek, H., 1992, "Fitting the Sunspot Cycles 10–21 by a Modified F-Distribution Density Function", *Solar Phys.*, **137**, 155–165. [DOI], [ADS] (Cited on pages 33 and 47.)

Ferreira, S.E. and Potgieter, M.S., 2004, "Long-Term Cosmic Ray Modulation in the Heliosphere", *Astrophys. J.*, **603**, 744–752. [ADS] (Cited on page 23.)

Feynman, J., 1982, "Geomagnetic and Solar Wind Cycles, 1900-1975", *J. Geophys. Res.*, **87**(A8), 6153–6166. [DOI], [ADS] (Cited on pages 21 and 50.)

Fligge, M. and Solanki, S.K., 1997, "Inter-cycle Variations of Solar Irradiance: Sunspot Areas as a Pointer", *Solar Phys.*, **173**, 427–439. [DOI], [ADS] (Cited on page 11.)

Forbush, S.E., 1954, "World-Wide Cosmic-Ray Variations, 1937–1952", *J. Geophys. Res.*, **59**, 525–542. [ADS] (Cited on page 23.)

Fröhlich, C. and Lean, J., 1998, "The Sun's Total Irradiance: Cycles, Trends and Related Climate Change Uncertainties since 1976", *Geophys. Res. Lett.*, **25**, 4377–4380. [DOI], [ADS] (Cited on page 15.)

Garcia, A. and Mouradian, Z., 1998, "The Gleissberg Cycle of Minima", *Solar Phys.*, **180**, 495–498. [DOI], [ADS] (Cited on page 43.)

Gleissberg, M.N., 1939, "A long-periodic Fluctuation of the Sun-spot Numbers", *Observatory*, **62**, 158–159. [ADS] (Cited on pages 43 and 48.)

Gnevyshev, M.N., 1963, "The corona and the 11-year cycle of solar activity", *Sov. Astron.*, **7**, 311–318. [ADS] (Cited on page 46.)

Gnevyshev, M.N., 1967, "On the 11-Years Cycle of Solar Activity", *Solar Phys.*, **1**, 107–120. [DOI], [ADS] (Cited on page 46.)

Gnevyshev, M.N., 1977, "Essential features of the 11-year solar cycle", *Solar Phys.*, **51**, 175–183. [DOI], [ADS] (Cited on page 46.)

Gnevyshev, M.N. and Ohl, A.I., 1948, "On the 22-year cycle of solar activity", *Astron. Zh.*, **25**, 18–20 (Cited on pages 43 and 48.)

Haigh, J.D., 2007, "The Sun and the Earth's Climate", *Living Rev. Solar Phys.*, **4**, lrsp-2007-2. URL (cited on 3 February 2010):
http://www.livingreviews.org/lrsp-2007-2 (Cited on page 5.)

Hale, G.E., 1908, "On the Probable Existence of a Magnetic Field in Sun-Spots", *Astrophys. J.*, **28**, 315–343. [DOI], [ADS] (Cited on page 17.)

Hale, G.E., Ellerman, F., Nicholson, S.B. and Joy, A.H., 1919, "The Magnetic Polarity of Sun-Spots", *Astrophys. J.*, **49**, 153–178. [DOI], [ADS] (Cited on pages 17 and 18.)

Harvey, K.L. and White, O.R., 1999, "What is solar cycle minimum?", *J. Geophys. Res.*, **104**(A9), 19,759–19,764. [DOI], [ADS] (Cited on page 27.)

Hathaway, D.H., 1996, "Doppler measurements of the Sun's meridional flow", *Astrophys. J.*, **460**, 1027–1033. [DOI], [ADS] (Cited on page 54.)

Hathaway, D.H. and Wilson, R.M., 2006, "Geomagnetic activity indicates large amplitude for sunspot cycle 24", *Geophys. Res. Lett.*, **33**, L18101. [DOI], [ADS] (Cited on page 50.)

Hathaway, D.H., Wilson, R.M. and Reichmann, E.J., 1994, "The Shape of the Sunspot Cycle", *Solar Phys.*, **151**, 177–190. [DOI], [ADS] (Cited on pages 33, 34, 35, 36, and 47.)

Hathaway, D.H., Wilson, R.M. and Reichmann, E.J., 1999, "A synthesis of solar cycle prediction techniques", *J. Geophys. Res.*, **104**(A10), 22,375–22,388. [DOI], [ADS] (Cited on pages 29, 43, and 50.)

Hathaway, D.H., Wilson, R.M. and Reichmann, E.J., 2002, "Group Sunspot Numbers: Sunspot Cycle Characteristics", *Solar Phys.*, **211**, 357–370. [ADS] (Cited on pages 10, 11, 31, 34, and 42.)

Hathaway, D.H., Nandy, D., Wilson, R.M. and Reichmann, E.J., 2003, "Evidence that a Deep Meridional Flow Sets the Sunspot Cycle Period", *Astrophys. J.*, **589**, 665–670. [DOI], [ADS] (Cited on page 36.)

Henney, C.J. and Harvey, J.W., 2002, "Phase Coherence of Solar Magnetic Activity", *Solar Phys.*, **207**, 199–218. [DOI], [ADS] (Cited on page 40.)

Hodgson, R., 1859, "On a Curious Appearance seen in the Sun", *Mon. Not. R. Astron. Soc.*, **20**, 15–16. [ADS] (Cited on page 18.)

Holland, R.L. and Vaughn, W.W., 1984, "Lagrangian Least-Squares Prediction of Solar Flux ($F_{10.7}$)", *J. Geophys. Res.*, **89**, 11–16. [DOI], [ADS] (Cited on page 14.)

Howe, R. Christensen-Dalsgaard, J., Hill, F., Komm, R., Schou, J., Thompson, M.J. and Toomre, J., 2007, "Temporal variations in the solar rotation at the bottom of the convection zone: The current status", *Adv. Space Res.*, **40**, 915–918. [ADS] (Cited on page 46.)

Howe, R., Christensen-Dalsgaard, J., Hill, F., Komm, R.W., Larsen, R.M., Schou, J., Thompson, M.J. and Toomre, J., 2000, "Dynamic Variations at the Base of the Solar Convection Zone", *Science*, **287**, 2456–2460. [DOI], [ADS] (Cited on page 46.)

Hoyt, D.V. and Schatten, K.H., 1998, "Group Sunspot Numbers: A New Solar Activity Reconstruction", *Solar Phys.*, **179**, 189–219. [ADS] (Cited on pages 10 and 42.)

Javaraiah, J., 2007, "North–south asymmetry in solar activity: predicting the amplitude of the next solar cycle", *Mon. Not. R. Astron. Soc.*, **377**, L34–L38. [DOI], [ADS], [astro-ph/0701923] (Cited on page 48.)

Keller, C.U. (NSO Staff), 1998, "SOLIS – A modern Facility for Synoptic Solar Observations", in *Cool Stars, Stellar Systems and the Sun: Tenth Cambridge Workshop*, (Eds.) Donahue, R.A., Bookbinder, J.A., Proceedings of a meeting held at Cambridge, Massachusetts, 15 – 19 July 1997, vol. 154 of ASP Conference Series, pp. 636–649, Astronomical Society of the Pacific, San Francisco. [ADS] (Cited on page 17.)

Lean, J., 1990, "Evolution of the 155 Day Periodicity in Sunspot Areas During Solar Cycles 12 to 21", *Astrophys. J.*, **363**, 718–727. [DOI], [ADS] (Cited on page 45.)

Legrand, J.-P. and Simon, P.A., 1985, "Some solar cycle phenomena related to the geomagnetic activity from 1868 to 1980. I. The shock events, or the interplanetary expansion of the toroidal field", *Astron. Astrophys.*, **152**, 199–204. [ADS] (Cited on page 21.)

Lockwood, M., Stamper, R. and Wild, M.N., 1999, "A doubling of the Sun's coronal magnetic field during the past 100 years", *Nature*, **399**, 437–439. [DOI], [ADS] (Cited on page 21.)

MacQueen, R.M., Eddy, J.A., Gosling, J.T., Hildner, E., Munro, R.H., Newkirk Jr, G.A., Poland, A.I. and Ross, C.L., 1974, "The Outer Solar Corona as Observed from Skylab: Preliminary Results", *Astrophys. J. Lett.*, **187**, L85–L88. [DOI], [ADS] (Cited on page 19.)

Masarik, J. and Beer, J., 1999, "Simulation of particle fluxes and cosmogenic nuclide production in the Earth's atmosphere", *J. Geophys. Res.*, **104**(D10), 12,099–12,111. [DOI], [ADS] (Cited on page 24.)

Maunder, E.W., 1890, "Professor Spoerer's Researches on Sun-spots", *Mon. Not. R. Astron. Soc.*, **50**, 251–252. [ADS] (Cited on pages 37 and 42.)

Maunder, E.W., 1903, "Spoerer's Law of Zones", *Observatory*, **26**, 329–330. [ADS] (Cited on page 13.)

Maunder, E.W., 1904, "Note on the Distribution of Sun-spots in Heliographic Latitude, 1874 to 1902", *Mon. Not. R. Astron. Soc.*, **64**, 747–761. [ADS] (Cited on pages 13 and 37.)

Mayaud, P.N., 1972, "The *aa* indices: a 100-year series characterizing the magnetic activity", *J. Geophys. Res.*, **77**, 6870–6874. [DOI], [ADS] (Cited on page 19.)

McKinnon, J.A., 1987, *Sunspot Numbers: 1610-1985 (based on The Sunspot-Activity in the Years 1610-1960, by Prof. M. Waldmeier, Copyright 1961, Swiss Federal Observatory, Zurich, Switzerland)*, UAG Reports UAG-95, National Geophysical Data Center, NOAA, Boulder, CO (Cited on page 25.)

McNish, A.G. and Lincoln, J.V., 1949, "Prediction of sunspot numbers", *Eos Trans. AGU*, **30**, 673–685 (Cited on page 47.)

Miklailutsa, V.P. and Makarova, V.V., 1994, "The Sector Structure of the Active Longitudes in Solar Cycles", *Solar Phys.*, **155**, 391–400. [ADS] (Cited on page 40.)

Mursula, K., Zieger, B. and Vilppola, J.H., 2003, "Mid-term Quasi-periodicities in Geomagnetic Activity During the Last 15 Solar Cycles: Connection to Solar Dynamo Strength", *Solar Phys.*, **212**, 201–207. [DOI], [ADS] (Cited on page 46.)

Newton, H.W. and Milsom, A.S., 1955, "Note on the observed differences in spottedness of the Sun's northern and southern hemispheres", *Mon. Not. R. Astron. Soc.*, **115**, 398–404. [ADS] (Cited on page 38.)

"Sunspot Number Data via FTP", project homepage, NOAA National Geophysical Data Center (NGDC). URL (cited on 3 February 2010):
http://www.ngdc.noaa.gov/stp/SOLAR/ftpsunspotnumber.html (Cited on page 10.)

Nordemann, D.J.R., 1992, "Sunspot Number Time Series: Exponential Fitting and Solar Behavior", *Solar Phys.*, **141**, 199–202. [ADS] (Cited on page 33.)

Noyes, R.W., 1982, *The Sun, Our Star*, The Harvard Books on Astronomy, Harvard University Press, Cambridge, MA (Cited on page 6.)

Ogurtsov, M.G., Nagovitsyn, Y.A., Kocharov, G.E. and Jungner, H., 2002, "Long-period cycles of the Sun's activity recorded in direct solar data and proxies", *Solar Phys.*, **211**, 371–394. [DOI], [ADS] (Cited on page 43.)

Ohl, A.I., 1966, "Forecast of sunspot maximum number of cycle 20", *Soln. Dannye*, (12), 84 (Cited on page 48.)

Parker, E.N., 1965, "The passage of energetic charged particles through interplanetary space", *Planet. Space Sci.*, **13**, 9–49. [DOI], [ADS] (Cited on page 23.)

Pulkkinen, T., 2007, "Space Weather: Terrestrial Perspectives", *Living Rev. Solar Phys.*, **4**, lrsp-2007-1. URL (cited on 3 February 2010):
http://www.livingreviews.org/lrsp-2007-1 (Cited on page 5.)

"Royal Greenwich Observatory – USAF/NOAA Sunspot Data", project homepage, NASA / Marshall Space Flight Center. URL (cited on 3 February 2010):
http://solarscience.msfc.nasa.gov/greenwch.shtml (Cited on page 13.)

Ribes, J.C. and Nesme-Ribes, E., 1993, "The solar sunspot cycle in the Maunder minimum AD 1645 to AD 1715", *Astron. Astrophys.*, **276**, 549–563. [ADS] (Cited on page 42.)

Rieger, E., Share, G.H., Forrest, D.J., Kanbach, G., Reppin, C. and Chupp, E.L., 1984, "A 154-day periodicity in the occurrence of hard solar flares?", *Nature*, **312**, 623–625. [DOI], [ADS] (Cited on page 45.)

Roy, J.-R., 1977, "The North–South Distribution of Major Solar Flare Events, Sunspot Magnetic Classes and Sunspot Areas (1955–1974)", *Solar Phys.*, **52**, 53–61. [DOI], [ADS] (Cited on page 37.)

Rozelot, J.P., 1994, "On the stability of the 11-year solar cycle period (and a few others)", *Solar Phys.*, **149**, 149–154. [DOI], [ADS] (Cited on page 43.)

Sawyer, C., 1968, "Statistics of Solar Active Regions", *Annu. Rev. Astron. Astrophys.*, **6**, 115–134. [DOI], [ADS] (Cited on page 40.)

Schatten, K.H. and Sofia, S., 1987, "Forecast of an exceptionally large even-numbered solar cycle", *Geophys. Res. Lett.*, **14**, 632–635. [DOI], [ADS] (Cited on page 50.)

Schatten, K.H., Scherrer, P., Svalgaard, L. and Wilcox, J.M., 1978, "Using dynamo theory to predict the sunspot number during solar cycle 21", *Geophys. Res. Lett.*, **5**, 411–414. [DOI], [ADS] (Cited on page 53.)

Scherrer, P.H., Bogart, R.S., Bush, R.I., Hoeksema, J.T., Kosovichev, A.G., Schou, J., Rosenberg, W., Springer, L., Tarbell, T.D., Title, A., Wolfson, C.J. and Zayer, I. (MDI Engineering Team), 1995, "The Solar Oscillations Investigation – Michelson Doppler Imager", *Solar Phys.*, **162**, 129–188. [DOI], [ADS] (Cited on page 18.)

Schwabe, H., 1844, "Sonnen-Beobachtungen im Jahre 1843", *Astron. Nachr.*, **21**(495), 233–236. [DOI], [ADS] (Cited on page 6.)

Sheeley Jr, N.R., 1991, "Polar Faculae: 1906–1990", *Astrophys. J.*, **374**, 386–389. [ADS] (Cited on page 17.)

Sheeley Jr, N.R., 2005, "Surface Evolution of the Sun's Magnetic Field: A Historical Review of the Flux-Transport Mechanism", *Living Rev. Solar Phys.*, **2**, lrsp-2005-5. URL (cited on 3 February 2010):
http://www.livingreviews.org/lrsp-2005-5 (Cited on page 43.)

"Solar Influences Data Analysis Center - SIDC", institutional homepage, Royal Observatory of Belgium. URL (cited on 3 February 2010):
http://sidc.oma.be/ (Cited on page 10.)

Solanki, S.K., Krivova, N.A., Schüssler, M. and Fligge, M., 2002, "Search for a relationship between solar cycle amplitude and length", *Astron. Astrophys.*, **396**, 1029–1035. [DOI], [ADS] (Cited on page 36.)

Solanki, S.K., Usoskin, I.G., Kromer, B., Schüssler, M. and Beer, J., 2004, "Unusual activity of the Sun during the previous 11,000 years", *Nature*, **431**, 1084–1087. [DOI], [ADS] (Cited on page 43.)

Spoerer, M.G., 1889, "Sur les différences que présentent l'hémisphère nord et l'hémisphère sud du soleil", *Bull. Astron. (Paris)*, **6**, 60–63. [ADS] (Cited on page 37.)

Stewart, J.Q. and Panofsky, H.A.A., 1938, "The Mathematical Characteristics of Sunspot Variations", *Astrophys. J.*, **88**, 385–407. [DOI], [ADS] (Cited on pages 33 and 47.)

Stuiver, M. and Quay, P.D., 1980, "Changes in Atmospheric Carbon-14 Attributed to a Variable Sun", *Science*, **207**, 11–19. [DOI], [ADS] (Cited on page 24.)

Suess, H.E., 1980, "The radiocarbon record in tree rings of the last 8000 years", *Radiocarbon*, **22**, 200–209 (Cited on page 44.)

Svalgaard, L., Cliver, E.W. and Le Sager, P., 2004, "IHV: a new long-term geomagnetic index", *Adv. Space Res.*, **34**, 436–439. [DOI], [ADS] (Cited on page 19.)

Svalgaard, L., Cliver, E.W. and Kamide, Y., 2005, "Sunspot cycle 24: Smallest cycle in 100 years?", *Geophys. Res. Lett.*, **32**, L01 104. [DOI], [ADS] (Cited on pages 53 and 54.)

Tapping, K.F. and Charrois, D.P., 1994, "Limits to the Accuracy of the 10.7 cm Flux", *Solar Phys.*, **150**, 305–315. [DOI], [ADS] (Cited on page 13.)

Thompson, J.R., 1993, "A technique for predicting the amplitude of the solar cycle", *Solar Phys.*, **148**, 383–388. [DOI], [ADS] (Cited on page 50.)

Tobias, S., Hughes, D. and Weiss, N., 2006, "Unpredictable Sun leaves researchers in the dark", *Nature*, **442**, 26. [DOI], [ADS] (Cited on page 55.)

Tousey, R., 1973, "The Solar Corona", in *Space Research XIII*, (Eds.) Rycroft, M.J., Runcorn, S.K., Proceedings of open meetings of working groups on physical sciences of the 15th plenary meeting of COSPAR, Madrid, Spain, 10 – 24 May, 1972, p. 713, Akademie-Verlag, Berlin. [ADS] (Cited on page 19.)

Usoskin, I.G., 2008, "A History of Solar Activity over Millennia", *Living Rev. Solar Phys.*, **5**, lrsp-2008-3. URL (cited on 3 February 2010): http://www.livingreviews.org/lrsp-2008-3 (Cited on page 44.)

Vitinskij, Y.I., 1976, "Forecast of the Height of Solar Cycle 21 Using methods Based on the Latitude Distribution of Sunspots", *Soln. Dannye*, (11), 59–63. [ADS] (Cited on page 36.)

Vonmoos, M., Beer, J. and Muscheler, R., 2006, "Large variations in the Holocene solar activity: Constraints from ^{10}Be in the Greenland Ice Core Project ice core", *J. Geophys. Res.*, **111**, A10105. [DOI], [ADS] (Cited on page 44.)

Waldmeier, M., 1935, "Neue Eigenschaften der Sonnenfleckenkurve", *Astron. Mitt. Zurich*, **14** (133), 105–130. [ADS] (Cited on pages 25, 33, and 34.)

Waldmeier, M., 1939, "Die Zonenwanderung der Sonnenflecken", *Astron. Mitt. Zurich*, **14**(138), 470–481. [ADS] (Cited on page 34.)

Waldmeier, M., 1955, *Ergebnisse und Probleme der Sonnenforschung*, Geest & Portig, Leipzig, 2nd edn. [ADS] (Cited on page 37.)

Waldmeier, M., 1957, "Der lange Sonnenzyklus", *Z. Astrophys.*, **43**, 149–160. [ADS] (Cited on page 38.)

Waldmeier, M., 1961, *The Sunspot-Activity in the Years 1610-1960*, Schulthess u. Co. / Swiss Federal Observatory, Zürich. [ADS] (Cited on page 25.)

Waldmeier, M., 1971, "The Asymmetry of Solar Activity in the Years 1959-1969", *Solar Phys.*, **20**, 332–344. [DOI], [ADS] (Cited on pages 37 and 38.)

Wang, Y.-M. and Sheeley Jr, N.R., 2003, "On the fluctuating component of the Sun's large-scale magnetic field", *Astrophys. J.*, **590**, 1111–1120. [DOI], [ADS] (Cited on page 46.)

Wang, Y.-M. and Sheeley Jr, N.R., 2009, "Understanding the geomagnetic precursor of the solar cycle", *Astrophys. J. Lett.*, **694**, L11–L15. [DOI], [ADS] (Cited on page 50.)

Webb, D.F. and Howard, R.A., 1994, "The solar cycle variation of coronal mass ejections and the solar wind mass flux", *J. Geophys. Res.*, **99**(A3), 4201–4220. [DOI], [ADS] (Cited on page 19.)

Willson, R.C., 1997, "Total Solar Irradiance Trend During Cycles 21 and 22", *Science*, **277**, 1963–1965. [DOI], [ADS] (Cited on page 15.)

Willson, R.C. and Hudson, H.S., 1988, "Solar luminosity variations in solar cycle 21", *Nature*, **332**, 810–812. [DOI], [ADS] (Cited on page 15.)

Wilson, R.M., 1987, "On the Distribution of Sunspot Cycle Periods", *J. Geophys. Res.*, **92**(A9), 10,101–10,104. [DOI], [ADS] (Cited on page 31.)

Wilson, R.M., 1988, "On the Long-term Secular Increase in Sunspot Number", *Solar Phys.*, **115**, 397–408. [DOI], [ADS] (Cited on page 42.)

Wilson, R.M., Hathaway, D.H. and Reichmann, E.J., 1998, "An estimate for the size of cycle 23 based on near minimum conditions", *J. Geophys. Res.*, **103**(A4), 6595–6603. [DOI], [ADS] (Cited on page 48.)

Wittmann, A.D. and Xu, Z.T., 1987, "A catalogue of sunspot observations from 165 BC to AD 1684", *Astron. Astrophys. Suppl.*, **70**, 83–94. [ADS] (Cited on page 6.)

Wolf, R., 1859, "Extract of a Letter from Prof. R. Wolf, of Zurich, to Mr. Carrington, dated Jan. 12, 1859", *Mon. Not. R. Astron. Soc.*, **19**, 85–86. [ADS] (Cited on page 25.)

Wolf, R., 1861, "Abstract of his latest Results", *Mon. Not. R. Astron. Soc.*, **21**, 77–78. [ADS] (Cited on page 7.)

Wolf, R., 1877, *Geschichte der Astronomie*, vol. 16 of Geschichte der Wissenschaften in Deutschland. Neuere Zeit, Oldenbourg, München. Related online version (cited on 9 February 2010): http://ebooks.ethbib.ethz.ch/fulltext/Rara/1681.pdf (Cited on page 6.)

Wolf, R., 1892, "Astronomische Mittheilungen, LXXIX", *Astron. Mitt. Zurich*, **79**, 317–364. [ADS] (Cited on page 27.)

Wolfer, A., 1903, "Astronomische Mitteilungen, XCIV", *Astron. Mitt. Zurich*, **94**, 97–150. [ADS] (Cited on page 27.)

Yeates, A.R., Nandy, D. and Mackay, D.H., 2008, "Exploring the Physical Basis of Solar Cycle Predictions: Flux Transport Dynamics and Persistence of Memory in Advection- versus Diffusion-dominated Solar Convection Zones", *Astrophys. J.*, **673**, 544–556. [DOI], [ADS] (Cited on page 54.)